JOURNAL OF BIOMOLECULAR STRUCTURE AND DYNAMICS
https://doi.org/10.1080/07391102.2020.1835726

Prevention of SARS-CoV-2 cell entry: insight from *in silico* interaction of drug-like alkaloids with spike glycoprotein, human ACE2, and TMPRSS2

Gideon A. Gyebi[a], Adegbenro P. Adegunloye[b], Ibrahim M. Ibrahim[c], Oludare M. Ogunyemi[a], Saheed O. Afolabi[d] and Olalekan B. Ogunro[e]

[a]Department of Biological Sciences, Salem University, Lokoja, Nigeria; [b]Faculty of Life Sciences, Department of Biochemistry, University of Ilorin, Ilorin, Nigeria; [c]Faculty of Sciences, Department of Biophysics, Cairo University, Giza, Egypt; [d]Faculty of Basic Medical Sciences, Department of Pharmacology and Therapeutics, University of Ilorin, Ilorin, Nigeria; [e]Department of Biological Sciences, KolaDaisi University, Ibadan, Nigeria

Communicated by Ramaswamy H. Sarma

ABSTRACT

COVID-19 is a respiratory disease caused by SARS-CoV-2, an enveloped positive sense RNA virus. The SARS-CoV-2 spike glycoprotein, *human* angiotensin-converting enzyme 2 (ACE2) and human transmembrane protease serine 2 (TMPRSS2) are essential for the host cell-mediated viral entry. Targeting these proteins represent viable options to stop the first stage of infection and transmission. Hence, 97 alkaloids from African medicinal plants with reported antiviral activity were evaluated for this purpose via *in silico* studies. These alkaloids were docked for their interactions with SARS-CoV-2 spike glycoprotein, ACE2, and TMPRSS2. Top 20 alkaloids with highest binding affinities were further screened for their interactions with spike glycoprotein of SARS-CoV and MERS-CoV, and with ACE2-SARS-CoV-2 receptor-binding domain complex (ACE2-RBD). The energy profiling, molecular dynamics simulation (MDS), binding free energy base on Molecular Mechanics/Generalized Born Surface Area (MMGBSA), clustering of MDS trajectories, and virtual physicochemical and pharmacokinetic screening of the best docked alkaloids were performed. Results revealed that more than 15 alkaloids interacted better than the reference compounds. 10–Hydroxyusambarensine and Cryptospirolepine were docked in a similar binding pattern to the S1-specificy pocket of TMPRSS2 as camostat (reference inhibitor). The strong binding affinities, stability of the alkaloid-protein complexes and amino acid interactions displayed by cryptospirolepine, 10-hydroxyusambarensine, and cryptoquindoline with important binding hotspots of the proteins suggest these alkaloids have the potential of altering the capacity of SARS-CoV-2 membrane mediated host cell entry. Further *in vitro* and *in vivo* evaluation of these "drug-like" alkaloids as potential inhibitors of coronavirus cell entry is proposed.

ARTICLE HISTORY
Received 15 May 2020
Accepted 7 October 2020

KEYWORDS
COVID-19; ACE2; TMPRSS2; spike glycoprotein; alkaloid

1. Introduction

Coronaviruses refer to a family of viruses that cause diverse forms of diseases in multiple animal hosts. Four main genera of coronaviruses – alpha, beta, gamma, and delta – infect animals but two of these genera, alpha and beta, transmit to humans (Paules et al., 2020). Human coronavirus (HCoV) causes respiratory tract complications which vary in severity. Prevalence of HCoVs and their association with upper and lower respiratory tract diseases ranges from 3.3% to 16% (Cabeça et al., 2013; Gaunt et al., 2010; Lu et al., 2012; Walsh et al., 2013). Alpha coronaviruses (HCoV-NL63 and HCoV-229E) and beta coronaviruses (HCoV-OC43 and HCoV-HKU1) are prevalent in human population and responsible for mild respiratory illnesses such as sore throat, cough, and common cold (Lu et al., 2012; Walsh et al., 2013), while beta coronaviruses like MERS-CoV (Middle East respiratory syndrome coronavirus), SARS-CoV (severe acute respiratory syndrome coronavirus), and SARS-CoV-2 (severe acute respiratory syndrome coronavirus 2) are rarer in human but more deadly (Letko et al., 2020). MERS-CoV, SARS-CoV, and SARS-CoV-2 are believed to have initially transmitted from a natural host, purported to be bat, via intermediate mammalian hosts to humans (Al-Tawfiq and Memish, 2014; Bolles et al., 2011; Zhou et al., 2020). The novel human coronavirus, SARS-CoV-2, was first identified in Wuhan, China in the year 2019 (WHO, 2020) and was reported as the causative agent of COVID-19 (coronavirus disease 2019).

SARS-CoV-2, an enveloped positive-sense RNA virus (Gorbalenya et al., 2020), utilizes its spike glycoprotein for receptor recognition and membrane fusion to initiate infection (Gallagher and Buchmeier, 2001; Simmons et al., 2013). The S_1 subunit of coronavirus spike glycoprotein contains the receptor binding domain (RBD), which binds to the peptidase domain (PD) of host cell angiotensin-converting enzyme 2 (ACE2) (Li et al., 2005), while S_2 subunit of the spike glycoprotein ensures membrane fusion with host cell (Tong, 2009). The human ACE2 is a type I integral membrane glycoprotein whose biological function is to process angiotensin, a peptide hormone that modulates vasoconstriction and blood pressure, into its matured form. But ACE2 is hijacked by some coronaviruses, like SARS-CoV and SARS-CoV-2, as entry point to host

CONTACT Gideon Ampoma Gyebi gideonagyebi@gmail.com Department of Biological Sciences, Salem University, Lokoja, Nigeria.

cell (Hoffmann et al., 2020). Relative to SARS-CoV, SARS-CoV-2 is believed to bind human ACE2 more efficiently, thereby increasing its chance of human to human transmission (Wan et al., 2020). In addition, SARS-CoV-2 just like SARS-CoV, utilizes host cell transmembrane protease serine 2 (TMPRSS2) to cleave its spike glycoprotein (Glowacka et al., 2011; Heurich et al., 2014; Hoffmann et al., 2020; Shulla et al., 2011) to ensure the fusion of host cell and virus membranes (Hoffmann et al., 2020). These interactions of SARS-CoV-2 spike glycoprotein with ACE2 and TMPRSS2 ensure the entry of the viral RNA genome into the host cell, where viral replication takes place. Both ACE2 and TMPRSS2 are well expressed in nasal and bronchial epithelium (Bertram et al., 2012).

Potential therapeutic approaches to curtail COVID-19 include development of SARS-CoV-2 spike glycoprotein-based vaccine; usage of transmembrane protease serine 2 (TMPRSS2) inhibitor to block the cleavage of the spike glycoprotein; usage of anti-ACE2 peptides or antibody to block ACE2 receptor surface; and introduction of soluble form of ACE2 to competitively bind with SARS-CoV-2, slow down viral entry into cells, and protect the lung from injury through its unique enzymatic function (Zhang et al., 2020). Computational techniques have been applied for virtual screening of several FDA approved drugs (Elmezayen et al., 2020; Lobo-Galo et al., 2020), natural agents (Aanouz et al., 2020), and repurposing of clinically approved antiviral drugs (Adeoye et al., 2020; Boopathi et al., 2020; Hendaus, 2020; Khan et al., 2020; Muralidharan et al., 2020).

Exploration of natural products presents the option of identifying compounds with minimal side effects. Alkaloids are secondary metabolites of plants used to manage diverse diseases. Given the antiviral potentials of alkaloids from Africa medicinal plants (Dhama et al., 2018; Kudi and Myint, 1999; Meyer et al., 1997; Ogbole et al., 2018), this research seeks to investigate the potentials of alkaloids to interact and alter binding function of coronavirus spike glycoprotein, block the receptor function of ACE2 and/or inhibit cleavage function of TMPRSS2. These disruptions could serve to prevent SARS-CoV-2 binding and fusion to cell, and consequently prevent infection of cells and viral replication.

2. Materials and methods

2.1. Protein preparation

The crystal structures of proteins for the docking studies were retrieved from Protein Databank (http://www.rcsb.org) with their various identification codes: ACE2 (1R42) (Towler et al., 2004); TMPRSS2 (2OQ5) (Kyrieleis et al., 2007); SARS-CoV-2 chimeric receptor-binding domain complexed with ACE2 tagged as ACE2-RBD (6VW1) (Shang et al., 2020); SARS-CoV-2 spike glycoprotein (6VSB) (Wrapp et al., 2020); SARS-CoV spike glycoprotein (5X5B) (Yuan et al., 2017); and MERS-CoV spike glycoprotein (5X5C) (Yuan et al., 2017). All the crystal structures were prepared by removing existing ligands and water molecules while missing hydrogen atoms were added using Autodock version 4.2 program (Scripps Research Institute, La Jolla, CA). Thereafter, nonpolar hydrogens were merged while polar hydrogens were added to each protein. The process was repeated for each protein and subsequently saved into dock-able PDBQT format.

2.2. Ligand preparation

Structure Data Format (SDF) structures of reference inhibitors (MLN-4760, N-Acetyl-D-Glucosamine, Camostat, and Nafamostat) and 97 alkaloids reportedly present in African plants were retrieved from the PubChem database (www.pubchem.ncbi.nlm.nih.gov), while compounds that were not available on the database were drawn with Chemdraw version 19, and converted to mol2 chemical format using Open babel (O'Boyle et al., 2011). Polar hydrogen charges of the Gasteiger-type were assigned while the nonpolar hydrogen molecules were merged with the carbons, and the internal degrees of freedom and torsions were set to zero. The ligand molecules were then converted to dock-able format using Autodock tools.

2.3. Molecular docking

The initial virtual screening of the alkaloids for active regions of the human host cell receptor, protease and the coronaviruses spike glycoprotein, were carried out using AutoDock vina (Trott and Olson, 2010), and validated with BINDSURF (https://bio-hpc.ucam.edu/achilles/) (Sánchez-Linares et al., 2012). AutoDock vina provides a one step and faster docking analysis which relies on both empirical and knowledge-based scoring functions, for this reason it was selected for the initial virtual screening. The estimated inhibition constant for the top-ranked alkaloids and reference compounds was calculated with AutoDock 4.2 (Morris et al., 2009). Twenty-five million energy evaluations were performed for each compound with a total of ten runs using AutoDock 4.2. Lamarckian Genetic Algorithm was used and Gasteiger partial charges were added to the proteins. PDBQT form of each protein and ligand were used for exhaustive docking calculations to find the spots with best binding affinities. The pose with the best affinity was taken as the representation of the cluster. The top 20 alkaloids with higher binding affinity for ACE2 were further docked with the complex formed between ACE2 and SARS-CoV-2 spike glycoprotein receptor-binding domain (ACE2-RBD). Also, these top 20 alkaloids were docked with the spike glycoproteins of SARS-CoV and MERS-CoV. The molecular interactions between these alkaloids and proteins were viewed with Discovery Studio Visualizer version 16.

2.4. Energy profile calculations

The energy profiles of the ligand-protein complex in the selected clusters with the best docked poses were calculated by BINDSURF. The number of poses and best poses in the selected clusters from the population cluster for each docked ligand and the binding coordinates in the cluster were calculated by the clustering tool.

2.5. Molecular dynamics simulation

Molecular Dynamics Simulation (MDS) using NAMD software (Phillips et al., 2005) was done on the resulted complexes

from AutoDockVina docking step. The files required for the MDS were prepared using CHARMM-GUI web server (Brooks et al., 2009; Lee et al., 2016). Each complex was minimized for 10,000 steps then a production run for 100 ns was performed. The simulation temperature was set at 310 K, and salt concentration was set at physiological concentration of 0.154 M NaCl.

The results from the MDS were analyzed using VMD TK console scripts for calculation of Backbone-Root Mean Square Deviation (RMSD), Per residue Root Mean Square Fluctuations (RMSF), Radius of Gyration (RoG), and Surface Accessible Surface Area (SASA) (Humphrey et al., 1996). In addition, Molecular Mechanics/Generalized Born Surface Area (MM/GBSA) (Miller et al., 2012) calculation was performed using AmberTools 20 (Case et al., 2020). MDS Trajectories were clustered automatically using TTClust Version 4.7.2 by utilizing the elbow method to calculate the number of clusters and a representative structure for each cluster was produced (Tubiana et al., 2018). Following that was the analysis of the representative structures using Protein Ligand Interaction Profiler (PLIP) webserver to know the types and number of bonds that participated in the interaction (Salentin et al., 2015).

2.6. Physicochemical and pharmacokinetic study

The alkaloids that demonstrated highest binding affinities to the proteins were subjected to Lipinski filter to predict their membrane permeability and ease of intestinal absorption via passive diffusion. To pass this test, the alkaloids were expected not to violate more than one criteria for drug-likeness of Lipinski's rule of five: octanol-water partition coefficient (log P) $\leq$5; molecular mass $\leq$500; hydrogen bond donors (OH + NH count) $\leq$5; and hydrogen bond acceptors (O + N atom count) $\leq$10 (Lipinski et al., 1997). The pharmacokinetic studies were performed with the SDF file and canonical SMILES of the selected alkaloids. The predicted absorption, distribution, metabolism, excretion, and toxicity (ADMET) studies were analyzed using the admetSAR webserver (Cheng et al., 2012).

3. Results

3.1. Molecular docking

The screened 97 alkaloids from African medicinal flora demonstrated varying degrees of binding with SARS-CoV-2 spike glycoprotein, human ACE2, and protease TMPRSS2 (Table S1, Supporting material). From the docking scores obtained from the analysis, ranking based on negative low value of binding free energy, and binding orientation in the respective proteins, a hit list of top 20 alkaloids was defined. The binding energies of alkaloids with highest binding affinities for complex formed between ACE2 and SARS-CoV-2 spike glycoprotein receptor-binding domain (ACE2-RBD) are presented in Table 1. The binding energies of alkaloids with highest binding affinities for spike glycoproteins of SARS-CoV-2, SARS-CoV, and MERS-CoV are presented in Table 2, while the estimated inhibition constant of the three top-ranked alkaloids with highest binding affinities for ACE2, TMPRSS2, and SARS-CoV-2 spike glycoprotein is presented in Table 3.

The results from this study revealed that MLN-4760 and N-Acetyl-d-glucosamine (reference inhibitors) interacted with human ACE2 with binding energy of −7.0 and −5.6 Kcal/mol and estimated inhibition constant of 25.62 and 65.02 μM, respectively (Tables 1 and 3). It was observed that all the top 20 alkaloids interacted with ACE2 with binding affinity higher than the two reference inhibitors used in this study. Cryptospirolepine, 10–hydroxyusambarensine, and strychnopentamine showed the best binding to ACE2 with energies of −10.7, −10.4, and −9.9 Kcal/mol and estimated inhibition constant of 2.67, 5.81, and 4.45 μM, respectively (Tables 1 and 3).

Base on the estimated inhibition constant, the 3 top-ranked alkaloids especially cryptospirolepine had lower values than the reference compounds (MLN-4760 and N-Acetyl-d-glucosamine). Furthermore, cryptospirolepine, 10–hydroxyusambarensine, and chrysopentamine showed the best binding affinities to the ACE2-RBD with energies of −10.7, −10.5, and −10.5 Kcal/mol, respectively (Table 1).

Fifteen of the top-ranked alkaloids interacted with TMPRSS2 with binding affinities better than that camostat (–7.6 Kcal/mol), a reference inhibitor of TMPRSS2. The interaction of 10–hydroxyusambarensine, cryptospirolepine, and cryptoquindoline to TMPRSS2 demonstrated highest binding affinities with energies of −10.4, −9.9, and −9.7 Kcal/mol (Table 1). Though the estimated inhibition constant of camostat for TMPRSS2 (1.56 μM) was lower compared to these 3 top-ranked alkaloids (Table 3).

The result also revealed that nafamostat, the reference inhibitor for spike glycoprotein, had better binding tendency to the spike glycoprotein of SARS-CoV and MERS-CoV than SARS-CoV-2. Also, more than ten of the top-ranked alkaloids have higher binding affinities to the spike glycoproteins than nafamostat (Table 2). The alkaloids, cryptospirolepine, isocryptolepine, and cryptoquindoline interacted with the spike glycoprotein of SARS-CoV-2 with better binding affinities and lower estimated inhibition constant than the reference compound (Tables 2 and 3). Cryptospirolepine and 10–hydroxyusambarensine demonstrated highest affinities to the spike glycoprotein of SARS-CoV and MERS-CoV (Table 2).

3.2. Interaction of alkaloids with amino acid residues of target proteins

The alkaloids with the highest binding affinities interacted with various the amino acid residues of human ACE2 and TMPRSS2, and these are represented in Table 4. Likewise, the amino acid residues of spike glycoprotein of SARS-CoV-2, SARS-CoV, and MERS-CoV interacted with top-binding alkaloids as presented in Table 5.

The interacted residues of ACE2 and TMPRSS2 with respective ligand groups were majorly through hydrophobic and hydrogen bond interactions (Table 4). Few hydrogen bonds below bond distance of 3.40 Å were observed with coronaviruses spike glycoproteins (Table 5).

The ligand-protein binding interaction showed that MLN-4760 was docked into the N terminus- and zinc-containing

Table 1. Binding energies of reference inhibitors and top 20 bioactive alkanoids with human Angiotensin-Converting Enzyme 2 (ACE2), Transmembrane Protease Serine 2 (TMPRSS2), and ACE2-Spike Receptor Binding Domain complex (ACE2-RBD).

				Binding energies (kcal/mol)					
				ACE2		TMPRSS2		ACE2-RBD	
S/No	Plant species (Family)	Class of compound	Compounds	Vina	Bindsurf	Vina	Bindsurf	Vina	Bindsurf
R1			MLN-4760	−7.0	7.2	ND	ND	ND	ND
R2			N-Acetyl-d-glucosamine	−5.6	−5.7	ND	ND	ND	ND
R3			Camostat	ND	ND	−7.6	−7.8	ND	ND
1	Cryptolepis sanguinolenta (Periplocaceae)	Cryptolepines	Cryptospirolepine	**−10.7**	**−10.8**	**−9.9**	**−10.2**	**−10.7**	−10.9
2	*Strychnos usambarensis* (Loganiaceae)	Indole alkaloids	10-Hydroxyusambarensine	**−10.4**	**−10.3**	**−10.4**	**−10.7**	**−10.5**	**−9.9**
3	*Strychnos usambarensis* (Loganiaceae)	Indole alkaloids	Strychnopentamine	**−9.9**	**−10.3**	−8.8	−8.9	−8.4	**−9.8**
4	Cryptolepis sanguinolenta (Periplocaceae)	Cryptolepines	Biscryptolepine	−9.8	−9.9	−8.9	−8.9	−10.1	−9.9
5	Cryptolepis sanguinolenta (Periplocaceae)	Cryptolepines	Cryptoquindoline	−9.7	−9.9	**−9.7**	**−9.9**	−9.9	−9.8
6	*Strychnos usambarensis* (Loganiaceae)	Indole alkaloids	Isostrychnopentamine	−9.5	−9.8	−8.7	−8.8	−9.2	−9.8
7	*Strychnos usambarensis* (Loganiaceae)	Indole alkaloids	Chrysopentamine	−9.4	−9.7	−8.6	−8.9	**−10.5**	−8.8
8	Triphyophyllum peltatum,	Naphthoisoquinolines	Jozipeltine A	−9.3	−9.7	−8.4	−8.7	−10.4	−8.9
9	*Monodora angolensis* (Annonaceae)	Indole alkaloids	Annonidine F	−9.0	−9.3	−7.8	−7.9	−9.2	−8.8
10	Atalantia monophylla Corrêa	Acridone alkaloid	Atalaphylline	−8.8	−8.9	−7.9	−7.6	−8.2	−8.6
11	Corydalis saxicola Bunting	Protoberberine-type	Coptisine	−8.7	−8.9	−8.2	−8.6	−8.7	−8.5
12	*Triphyophyllum peltatum* (Dioncophyllaceae)	Naphthoisoquinolines	Dioncophylline B	−8.6	−8.9	−7.7	−7.8	−8.6	−8.6
13	Corydalis saxicola Bunting	Protoberberine-type	dehydroapocavidine	−8.6	−8.7	−7.6	−7.9	−7.8	−8.4
14	*Fagara zanthoxyloides* (Rutaceae)	Indole alkaloids	Alstonine	−8.5	−8.8	−7.9	−7.8	−8.9	−8.6
15	*Triphyophyllum peltatum* (Dioncophyllaceae)	Naphthoisoquinolines	5′-*O*-Demethyl-dioncophylline A	−8.5	−8.5	−7.3	−7.6	−8.6	−7.9
16	*Triphyophyllum peltatum* (Dioncophyllaceae)	Naphthoisoquinolines	Dioncophylline A	−8.5	−8.9	−7.0	−7.4	−8.3	−8.3
17	*Glossocalyx brevipes* (Siparunaceae)	Indole alkaloids	Liriodenine	−8.4	−8.7	−7.3	−7.8	−8.6	−8.1
18	Camptotheca acuminate Decaisne	Quinoline	Camptothecin	−8.4	−8.9	−8.1	−8.8	−7.8	−8
19	Magnolia gradiflora	Aporphine	Lanuginosine.	−8.4	−8.8	−7.5	−7.9	−8.5	−8.5
20	Rhigiocarya racemifera	Oxoaporphine	Ancistrocladidine	−8.4	−8.9	−7.5	−7.5	−8.6	−8

R1, R2, and R3 are reference inhibitors. Values in bold are for alkaloids with highest binding affinities for the corresponding proteins.
ND = not determined.

Table 2. Binding energies of reference inhibitor and top 20 bioactive alkaloids from African plants with the spike glycoprotein of coronaviruses.

				Binding energies (kcal/mol)					
				SARS-CoV-2		SARS-CoV		MERS-CoV	
S/No	Plant species (Family)	Class of compound	Compounds	Vina	Bindsurf	Vina	Bindsurf	vina	Bindsurf
R1			Nafamostat	**−7.0**	**−7.2**	**−8.5**	**−8.7**	**9.7**	**9.6**
1	Cryptolepis sanguinolenta (Periplocaceae)	Cryptolepines	Cryptospirolepine	**−10.6**	−10.9	**−12.0**	**−12.1**	**−11.3**	**−11.4**
2	Cryptolepis sanguinolenta (Periplocaceae)	Cryptolepines	Isocryptolepine	**−9.7**	**−9.9**	−8.6	−8.8	−9.1	−9.2
3	Cryptolepis sanguinolenta (Periplocaceae)	Cryptolepines	Cryptoquindoline	**−9.5**	**−9.8**	−9.7	−9.5	−10.1	−10.4
4	*Strychnos usambarensis* (Loganiaceae)	Indole alkaloids	10 –Hydroxyusambarensine	−9.4	−9.9	**−10.0**	**−10.1**	**−11.4**	**−11.1**
5	*Fagara zanthoxyloides* (Rutaceae)	Indole alkaloids	Fagaronine	−9.3	−9.8	−7.4	−7.6	−8.2	−8.6
6	Triphyophyllum peltatum,	Naphthoisoquinolines	Jozipeltine A	−9.3	−9.8	−8.8	−8.8	−9.4	−9.3
7	*Triphyophyllum peltatum* (Dioncophyllaceae)	Naphthoisoquinolines	5′–*O*–Demethyl–dioncophylline A	−8.7	−8.8	−7.5	−7.2	−8.3	−8.6
8	*Strychnos usambarensis* (Loganiaceae)	Indole alkaloids	Chrysopentamine	−8.6	−8.9	−9.0	−9.1	−10.3	−10.1
9	*Monodora angolensis* (Annonaceae)	Indole alkaloids	Annonidine F	−8.4	−8.8	−8.3	−8.5	−10.0	−10.2
10	*Triphyophyllum peltatum* (Dioncophyllaceae)	Naphthoisoquinolines	Dioncopeltine A	−8.3	−8.6	−7.5	−7.6	−9.2	−9.9
11	*Strychnos usambarensis* (Loganiaceae)	Indole alkaloids	Isostrychnopentamine	−8.2	−8.5	−8.6	−8.7	−9.7	−9.8
12	Sida acuta (Malvaceae)	Cryptolepines	Cryptolepine	−8.2	−8.6	−7.2	−7.4	−9.7	−9.3
13	*Ancistrocladus tanzaniensis* (Acistrocladaceae)	Naphthoisoquinolines	Ancistrotanzanine C	−8.1	−8.4	−7.9	−7.0	9.3	9.2
14	Cryptolepis sanguinolenta (Periplocaceae)	Cryptolepines	Quindoline	−8.1	−8.6	−7.2	−7.8	−9.2	−9.7
15	*Strychnos usambarensis* (Loganiaceae)	Indole alkaloids	Strychnopentamine	−7.9	−7.9	−8.7	−8.3	−9.4	−9.4
16	*Ancistrocladus robertsoniorum* (Acistrocladaceae)	Naphthoisoquinolines	Ancistrobertsonine A	−7.9	−8.3	−8.0	−8.5	−7.5	−7.7
17	*Ancistrocladus robertsoniorum* (Acistrocladaceae)	Naphthoisoquinolines	Ancistrobertsonine B	−7.9	−8.1	−8.1	−8.0	−8.0	−8.8
18	*Ancistrocladus tanzaniensis* (Acistrocladaceae)	Naphthoisoquinolines	Ancistrocladidine	−7.9	−8	−7.5	−7.3	−8.5	−8.9
19	*Ancistrocladus tanzaniensis* (Acistrocladaceae)	Naphthoisoquinolines	Ancistrotectorine	−7.9	−8.5	−7.2	−7.2	−8.1	−8.3
20	*Triphyophyllum peltatum* (Dioncophyllaceae)	Naphthoisoquinolines	Dioncophylline A	−7.9	−8	−7.4	−7.7	−9.1	−9.8

R1 is reference inhibitor. Values in bold are for alkaloids with highest binding affinities for the corresponding proteins.

Table 3. Inhibition constant (Ki) of 3 top-ranked alkaloids with highest affinities for ACE2, TMPRSS2 and SARS-COV-2 spike glycoprotein.

		Inhibition constant (μM)		
S/No	Compounds	ACE2	TMPRSS2	SARS-COV-2 S glycoprotein
R1	MLN-4760	25.62	ND	ND
R2	*N*-Acetyl-d-glucosamine	65.02	ND	ND
R3	Camostat	ND	1.56	ND
R4	Nafamostat	ND	ND	63.03
1	Cryptospirolepine	2.67	6.55	23.21
2	10 -Hydroxyusambarensine	5.81	3.20	ND
3	Strychnopentamine	4.45	ND	ND
4	Isocryptolepine	ND	ND	18.11
5	Cryptoquindoline	ND	3.40	15.80

R1, R2, R3, and R4 are reference inhibitors. ND = not determined.

Table 4. Interacting amino acid residues of human ACE2 and TMPRSS2 with the top-binding alkaloids from African plants.

Compound	Protein target	Residues involved in hydrophobic interactions (bond distance, Å)	Residues involved in hydrogen bonding (bond distance, Å)
MLN-4760	ACE2	ASP^{382} (4.33) HIS^{401} (2.17) PHE^{40} (4.7) PHE^{390} (5.04,4.20) ARG^{393}(5.45)	ASN^{394} (2.17) ALA^{348} (2.37) ASP^{382} (2.61) ASP^{350} (2.90) TRY^{385} (3.17)
N-acetyl-D-glucosamine		ND	LYS^{470} (2.13) ILE^{468} (2.87) TRP^{473}(2.23) PHE^{473} (3.18) ASN^{188} (2.97)
Cryptospirolepine		HIS^{378} (4.43) HIS^{401} (5.15) PHE^{40} (4.84) ARG^{393}(5.68)	ALA^{348} (2.83) ASN^{394} (3.18)
10-Hydroxyusambarensine		ALA^{348} (5.21) HIS^{378} (4.54) HIS^{401} (4.72) PHE^{40} (5.33) PHE^{390} (3.88)	PRO^{346} (2.32) GLU^{375} (2.77) ASN^{394} (1.98)
Camostat	TMPRSS2	ND	ARG^{41} (3.23, 3.57) SER^{195} (2.88) ALA^{190} (2.61) ASP^{189} TRP^{215} (2.90) GLN^{192} (2.76, 2.49)
Cryptospirolepine		SER^{151} (2.55) TYR^{149} (5.54, 5.26, 5.22) ILE^{75} (4.78)	SER^{151} (2.02, 4.03) HIS^{40} SER^{39} (4.10)
10-Hydroxyusambarensine		ALA^{190} (5.09) HIS^{96} (4.68) HIS^{57} (4.65) ARG^{41} (4.371) TRP^{215} (3.63) GLN^{192} (4.12) CYS^{191} (4.53)	SER^{195} (2.32) SER^{214} (2.72) ASP^{189} (2.62) ALA^{190}(2.27)

ACE2 = Angiotensin-Converting Enzyme 2; TMPRSS2 = Transmembrane protease serine 2.
ND = Not detected.

Table 5. Interacting amino acid residues of spike glycoprotein of coronaviruses with the top-binding alkaloids from African plants.

Compound	Coronavirus	Residues involved in hydrophobic interactions (bond distance, Å)	Residues involved in hydrogen bonding (bond distance, Å)
Nafamostat	SARS-Cov-2	THR^{286} (3.02) GLN^{218} (3.15) PHE^{220} (5.87)	LYS^{300} (3.36) SER^{297} (2.33)
Cryptospirolepine		VAL^{860} (5.12) LEU^{828} (4.12) THR^{732} (4.14) HIS^{1058} (5.01) PRO^{863} (4.11) PRO^{862} (3.80) ASP^{867} (2.90)	ND
Isocryptolepine		LYS^{417} (4.33) ARG^{403} (2.33) ILE^{418} (4.79) TYR^{453} (6.13)	(2.33)
Nafamostat	SARS-CoV	PRO^{575} (4.00, 5.39) SER^{574} (5.00) PHE^{558} (2.00) ASP^{560} (2.02) ASP^{554} (3.72)	ASP^{554} (2.51)
Cryptospirolepine		TYR^{300} (2.02) LEU^{948} (4.88, 5.78) PHE^{837} (5.79, 4.52, 3.75) LYS^{836} (5.38) ARG^{982} (4.64)	ND
10-Hydroxyusambarensine		THR^{535} (5.15, 5.38) PRO^{575} SER^{574} (3.95, 3.69, 4.76) PHE^{578} (4.31) CYS^{576} VAL^{308} (5.33)	THR^{535} (2.24) CYS^{576} (3.72)
Nafamostat	MERS-CoV	SER^{51} (3.48) HIS^{348} (5.43) HIS^{670} (4.12) ILE^{337} (5.37) PHE^{354} (3.89) LEU^{344} (5.12) ARG^{335} (5.07)	SER^{51} (1.95) ASN^{342} (2.67) HIS^{670} (2.80) HIS^{348} (3.55)
10-Hydroxyusambarensine		ASN^{342} (2.72) HIS^{348} (5.11, 4.88) HIS^{670} (5.19, 5.38) ILE^{337}(5.03, 5,08, 5.15) LEU^{344} (5.36, 5,35) LYS^{668} (4.25) LYS^{668} (4.42, 5.23) PHE^{341}(4.97)	SER^{51} (3.36, 4.13) PHE^{354} (2.72)
Cryptospirolepine		ILE^{337} (5.50) PHE^{354} (5.03) ASP^{49} (3.79)	GLN^{78} (4.05) SER^{51} (3.14)

ND = Not detected.

subdomain I of ACE2 (Figure 1(a) and 2), while N-acetyl-D-glucosamine interacted with the amino residues in the C terminus-containing subdomain II (Figure 1(b)). MLN-4760 had Pi-Alkyl interaction with Phe^{40}, Phe^{390}, and His^{401}, a carbon hydrogen interaction to Arg^{393}, a Pi-Anion interaction to Asp^{382}, while the remaining residue interacted via hydrogen bond (Figure 1(a)). N-Acetyl-D-glucosamine interacted solely via conventional hydrogen bond to the entire amino acid residue (Figure 1(b)). Cryptospirolepine the topmost docked alkaloid and 10-hydroxyusambarensine was docked into the subdomain I of ACE2 in a similar manner as MLN-4760 (Figures 1(c,d) and 2). Cryptospirolepine interacted via carbon and Pi-donor hydrogen bond to Ala^{348} and Arg^{393}, respectively. It further interacted via Pi-Pi stacking to Phe^{40} and His^{401} and via Pi-Alkyl interaction to Arg^{393} (Figure 1(c)). 10–hydroxyusambarensine interacted to Pro^{346}, Glu^{375}, and Asn^{394} via hydrogen bond. Ala^{348}, Asp^{382}, and Asp^{350} were seen in a carbon hydrogen interaction, while a Pi-Pi T-shaped interaction was observed between His^{401}, Phe^{40}, Phe^{390}, and 10–hydroxyusambarensine (Figure 1(d)).

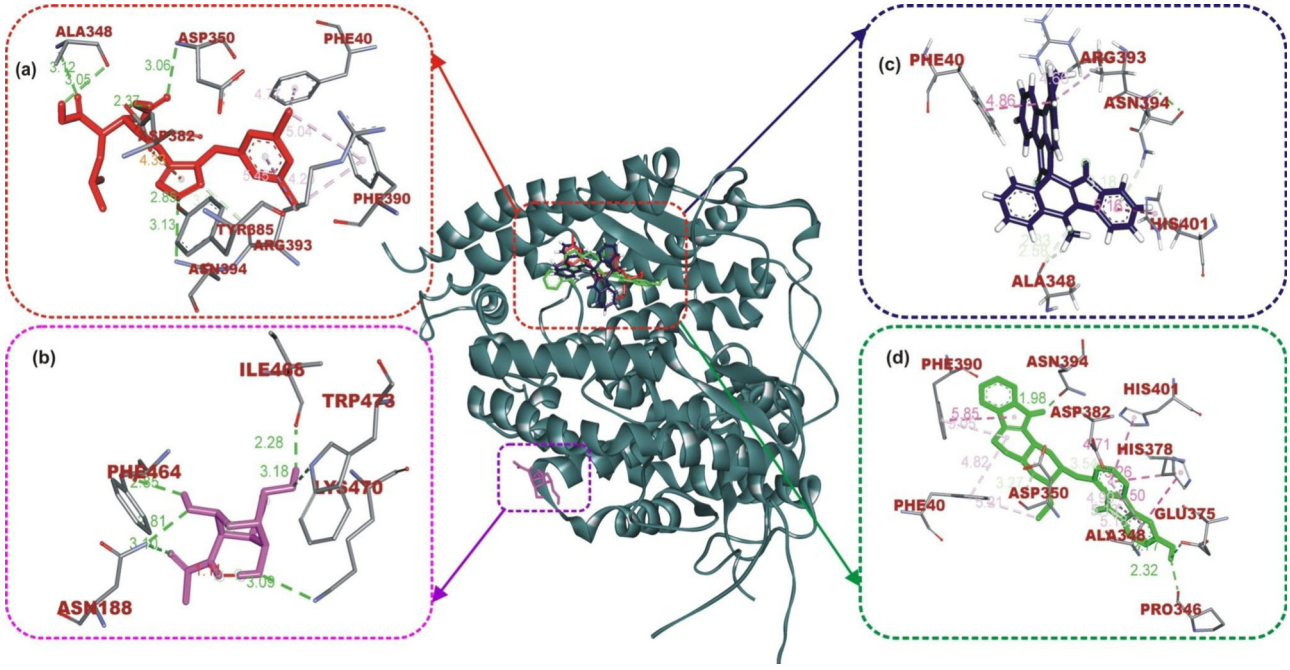

Figure 1. The interactive view of ligands in binding cavity of human ACE2. Ligands in sticks representation are presented by colors: (a) Red: MLN-4760, (b) Yellow: N-Acetyl-D-Glucosamine, (c) Blue: Cryptospirolepine, (d) Green: 10–Hydroxyusambarensine. Types of interactions are represented by Green-dotted lines: hydrogen bond interactions, light purple-dotted line: hydrophobic interactions (Pi-Alkyl, Alkyl, and pi-stacking) purple-dotted line: Pi-Pi T Shaped, yellow-dotted lines: Pi-sulfur interactions, pi-stacking interactions. Three-letter amino acids are in red color.

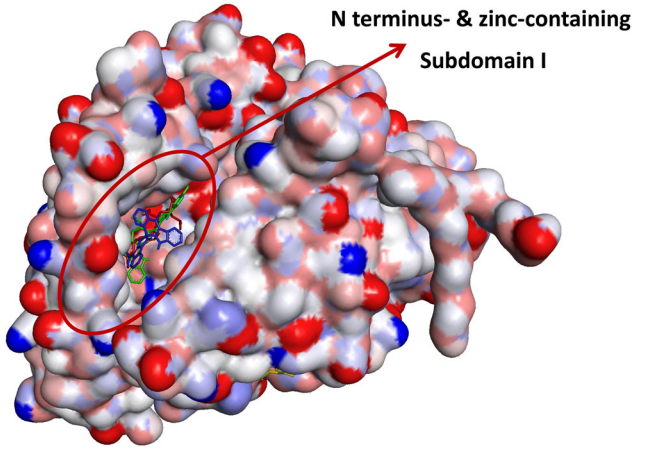

Figure 2. Surface view of ligands in binding cavity of human ACE2. (a) Green: 10–Hydroxyusambarensine; (b) Blue: Cryptospirolepine; and (c) Red: MLN-4760.

Camostat was docked into the S1-specificity pocket of TMPRSS2 (Figures 3(a) and 4). It interacted via carbon hydrogen interaction to Gln^{192} and via conventional hydrogen bond to five amino residues (Arg^{41}, Ser^{195}, Trp^{215}, Ala^{190}, and Asp^{189}) to TMPRSS2. The conventional hydrogen bond was formed in the direction of the guanidine group in this order: first ester bond, second ester bond, while the last three residues interacted with amidinonitrogen of guanidine group, respectively. The phenyl ring was responsible for the carbon hydrogen interaction with Gln^{192} (Figure 3(a)). While cryptospirolepine was docked close to the binding pocket, 10–hydroxyusambarensine (the highest docked alkaloid to TMPRSS2) was observed in the S_1-specificity pocked of TMPRSS2 (Figures 3(b) and 4), in a similar manner as camostat (Figure 3(a)). The difference observed was a Pi-Sigma interaction to Trp^{215}, an Amide-Pi Stacking to Cys^{191}, and an additional Pi-Alkyl interaction to His^{96} and His^{57} (Figure 3(c)).

Nafamostat, a reference inhibitor of the spike glycoprotein of SARS-CoV and MERS-CoV interacted with the spike glycoprotein of SARS-CoV-2 in a different manner. Nafamostat was docked into the subdomain SD1 and SD2 region of the S_1 subunit of SARS-CoV spike glycoprotein (Figure 5(a)). The same inhibitor was docked into to the N-terminal domain (NTD) region of the S_1 subunit of MERS-CoV spike glycoprotein (Figure 6(a)).

Cryptospirolepine with the highest binding affinity for SARS-CoV-2 spike glycoprotein also interacted with SARS-CoV and MERS-CoV spike glycoprotein in a different binding pattern. It formed mainly hydrophobic interaction with SARS-CoV-2 spike glycoprotein (Figure 7(b)) A Pi-Sigma interaction with Val^{860}, Leu^{828}, and Thr^{732} was observed between cryptospirolepine and SARS-CoV-2 spike glycoprotein, others include Pi-cation, Pi-alkyl, and Pi-Pi T-Shaped interactions with His^{1058}, Pro^{863}, and Pro^{862}, respectively (Figure 7(b)). Cryptospirolepine was docked into the S_2 subunit region of SARS-CoV spike glycoprotein. Most of the interaction was with amino acid residue in the heptad repeat (HR1) domain of the S_2 subunit (Figure 5(b)). Ala^{748} and Gln^{936} interacted via a carbon and Pi-donor hydrogen bond respectively; Arg^{996} and Gln^{939} and Asp^{932} via Pi-cation and Pi-anion, respectively (Figure 7(b) and Table 5). Cryptospirolepine was docked into the receptor-binding domain (RBD) of the S_1 Subunit of MERS-CoV spike glycoprotein through hydrophobic interaction. A P-Pi T-shaped, Pi-alkyl, Pi-anion interaction, and Pi-donor hydrogen bond was observed with Phe^{354}, Ile^{337}, Asp^{49}, and Ser^{51}, Gln^{78}, respectively (Figure 6(c)). 10-Hydroxyusambarensine interacted with the amino acid residue of the SD1 and SD2 region of the spike glycoprotein of SARS-CoV interacting via conventional carbon-hydrogen

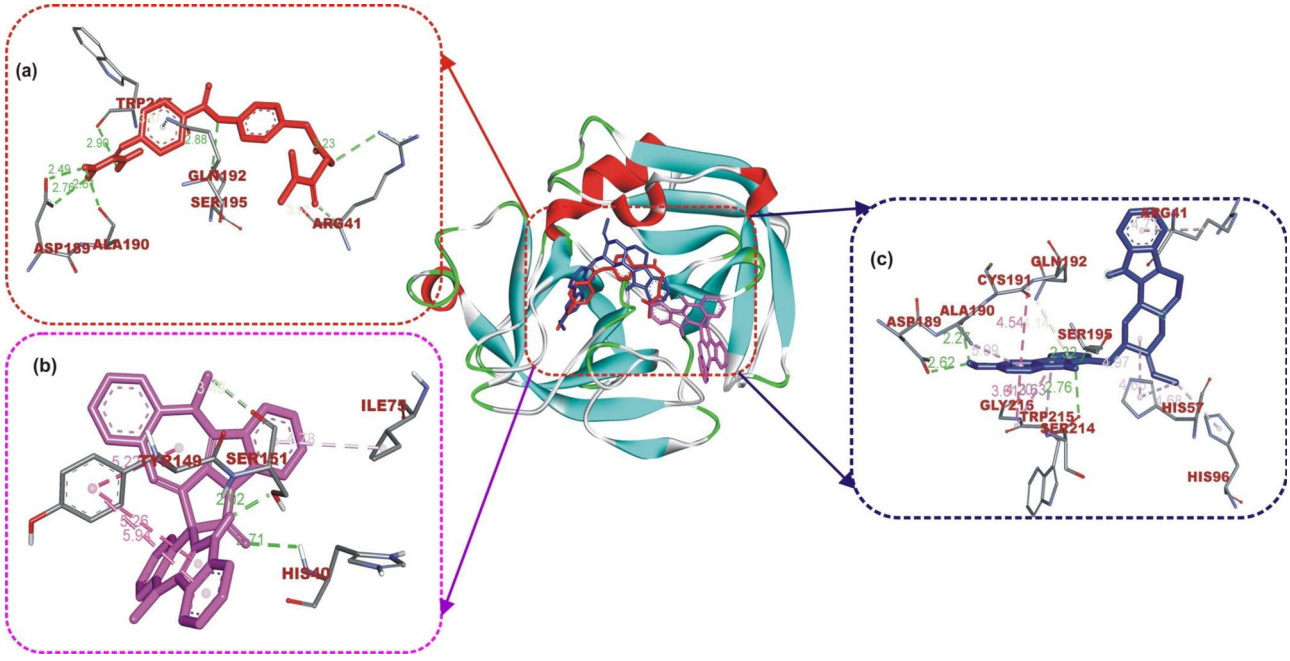

Figure 3. The interactive view of ligands in binding cavity of human TMPRSS2. Ligands in sticks representation are presented by colors: (a) Yellow: Camostat, (b) Black: Cryptospirolepine, (c) Green: 10-Hydroxyusambarensine. Types of interactions are represented by Green-dotted lines: hydrogen bond interactions, light purple-dotted line: hydrophobic interactions (Pi-Alkyl, Alkyl, and pi-stacking) purple-dotted line: Pi-Pi T Shaped, yellow-dotted lines: Pi-sulfur interactions, pi-stacking interactions. Three-letter amino acids are in red color.

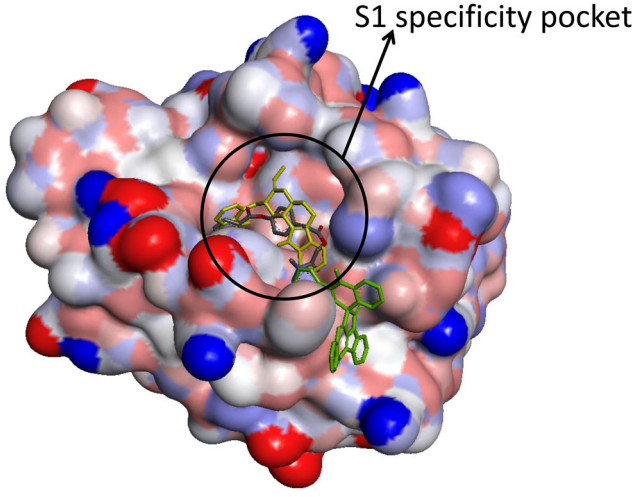

Figure 4. Surface view of ligands in binding cavity of human TMPRSS2. (a) Yellow: 10–Hydroxyusambarensine; (b) Black: Cryptospirolepine; (c) Green: Camostat.

interaction to Thr^{535} and Cys^{576} respectively; Amide-Pi stacking to SER^{574} and Pi-alkyl interaction to Pro^{575}, Phe^{578}, and Val^{308} (Figure 5(c)). The same ligand interacted to the spike glycoprotein of MERS-CoV via hydrogen bond to Ser^{51} and Phe^{354}; Pi-Pi T and Pi-Pi stacking Phe^{341} and His^{348}, respectively; Pi-alkyl and alkyl to His^{670}, Lys^{698}, and Leu^{344} Lys^{668}, respectively. The binding pattern exhibited by 10-hydroxyusambarensine was similar to that of Nafamostat to MERS-CoV.

3.3. Energy profile of best docked alkaloids to respective proteins

The number of poses and best poses in the selected clusters from the population cluster for each docked ligand and the binding coordinates in the cluster are shown in Table 6. The energy profiles of alkaloid-protein complex in the selected clusters with the best docked poses are shown in Figures 8–12. Gauss 1 (blue) and 2 (leaf green) bars represent the nonbonding interactions, red bar represents repulsion, light blue bar represents hydrophobic interaction, purple bar represents hydrogen bonds, light green bar represents rotational forces, while the black bar represents the total binding affinity which is a representative contribution of all bonding and nonbonding interactions between the alkaloids and the protein residues (Figures 8(a)–12(a)).

The contributions of the various type of interaction shows that of the total binding energy of −10.6 Kcal/mol exhibited by the binding of cryptospirolepine to the spike glycoprotein of SARS-CoV-2, −2.2 Kcal/mol was contributed by hydrophobic interaction, while the rest of the binding energy was contributed by nonbonding interaction mainly van der Waals, repulsive and rotational forces. A hydrophobic interaction and hydrogen bond energy of −0.5 and −1.5 Kcal/mol, respectively were contributed to the total binding energy between cryptospirolepine and spike glycoprotein of SARS-CoV. A hydrophobic interaction of −1.8, −1.6, and −2.3 Kcal/mol was contributed to the total binding energy of the spike glycoprotein of MERS-CoV, ACE2, and TMPRSS2 and respective alkaloids, while the rest of the energy was contributed by nonbonding interactions. The overall energy profile of the ligand-receptor complex of selected cluster with display of individual energetic contributions for each atom in the ligand are shown in Figures 8(b)–12(b). These reveal that the hydrogen bond energy that was contributed to the overall binding energy of MERS-CoV spike glycoprotein and respective ligand was mainly contributed by the interaction of oxygen atom with SER^{51} and PHE^{354}, while oxygen and nitrogen

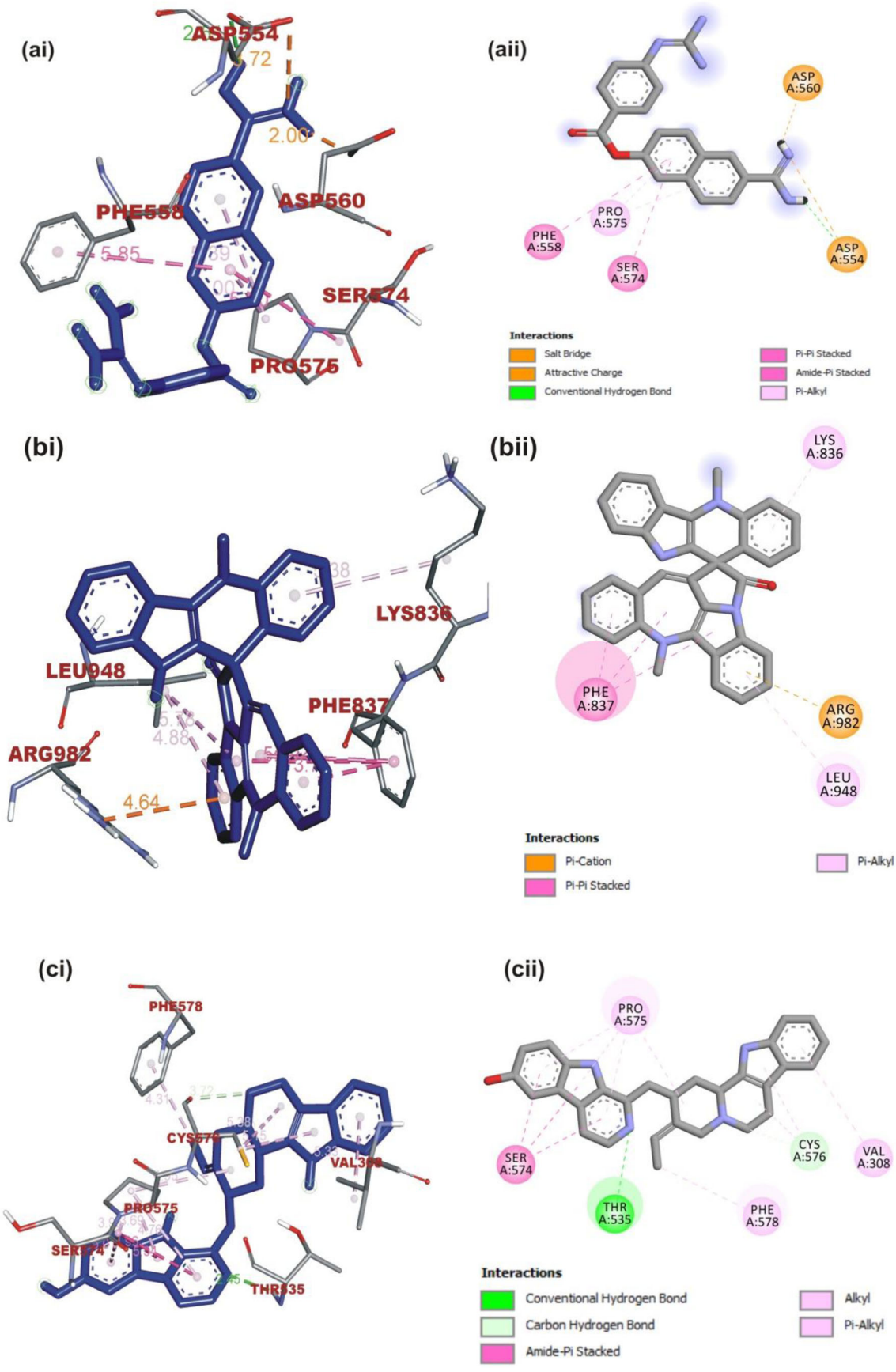

Figure 5. (i) 3D and (ii) 2D visualization of interacting amino acid residues of SARS-CoV spike glycoprotein with ligands: (a) Nafamostat, (b) Cryptospirolepine, (c) 10–Hydroxyusambarensine. *The ligands in stick representation are presented in (3D) as blue color while the (2D) as gray color*.

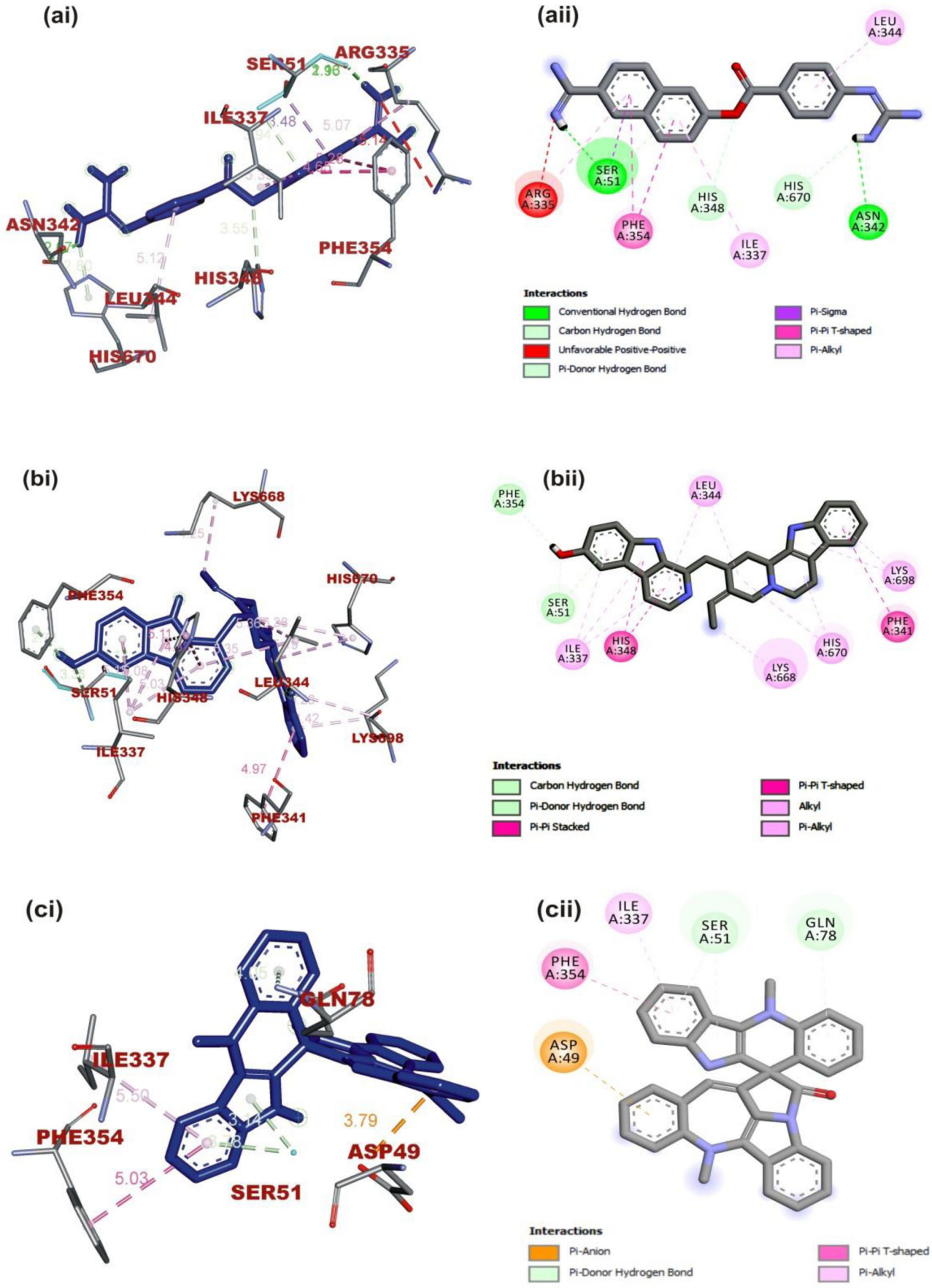

Figure 6. (i) 3D and (ii) 2D visualization of interacting amino acid residues of MERS-CoV spike glycoprotein with ligands: (a) Nafamostat, (b) 10–Hydroxyusambarensine, (c) Cryptospirolepine. *The ligands in stick representation are presented in (3D) as blue color while the (2D) as gray color*.

Table 6. The binding profile of the ligand in the selected cluster.

Receptor-ligand complex	Poses in Cluster	Best Pose	Binding site coordinate
Cryptospirolepine-6VSB	62	1547	214.25, 205.16, 213.99
Cryptospirolepine-5X5B	89	1746	13.00, −7.77, −9.61
10 –Hydroxyusambarensine-5X5C	87	338	34.87, −14.23, 0.60
Cryptospirolepine-IR42	102	28	65.46, 70.54, 30.12
Cryptospirolepine-2OQ5	92	132	(–2.85, 27.80, 22.38)

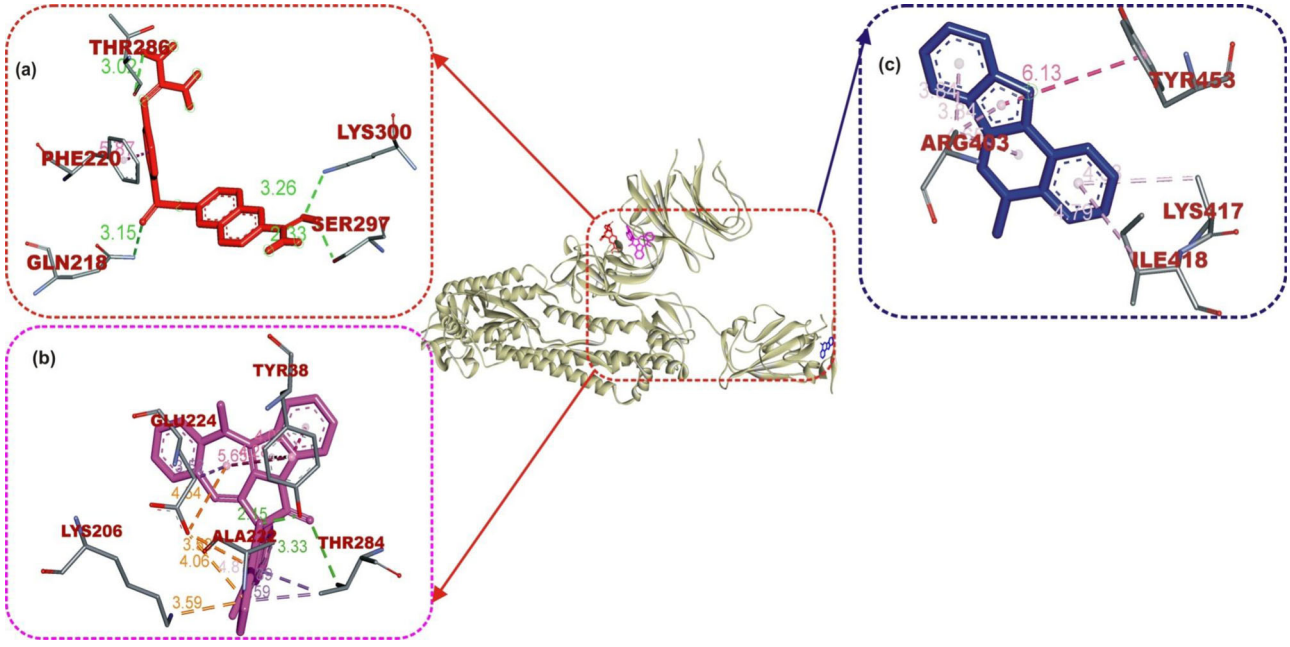

Figure 7. The interactive view of ligands in binding cavity of SARS-Cov-2 spike glycoprotein. Ligands in sticks representation are presented by colors: (a) Blue: Nafamostat, (b) Yellow: Cryptospirolepine, and (c) Red: Isocryptolepine. Types of interactions are represented by Green-dotted lines: hydrogen bond interactions, light purple-dotted line: hydrophobic interactions (Pi-Alkyl, Alkyl, and pi-stacking) purple-dotted line: Pi-Pi T Shaped, yellow-dotted lines: Pi-sulfur interactions, pi-stacking interactions. Three-letter amino acids are in red color.

atom contributed the total hydrogen bond energy of −1.4 Kcal/mol.

3.4. Results from molecular dynamics simulation

The complexes of best docked alkaloids to the target proteins were analyzed for MDS at 100 ns run. The results were analyzed using VMD Tk console scripts to calculate RMSD, SASA, RoG (Figure 13), and RMSF (Figure 14). TMPRSS2_Cryptospirolepine, and TMPRSS2_camostat complexes expressed similar RoG. The values of RoG of the S protein_3-Benzoylhosloppone complex, fluctuated about certain values towards the end of the run. The RMSD of the four protein-drug complexes has mean values of 3.36 Å, 1.99 Å, 11.9 Å, and 2.14 Å, and RMSF with mean values of 1.43 Å, 0.66 Å, 7.92 Å, and 0.73 Å for ACE2_(Cryptospirolepine), TMPRSS2_(Cryptospirolepine), S protein_3-Benzoylhosloppone, and TMPRSS2_camostat, respectively. The RMSF results for each protein-drug complex shows spikes at the end, which corresponds to the motion of the terminals (Figure 14).

Molecular Mechanics/Generalized Born Surface Area (MMGBSA) algorithm implemented in AmberTools 20 was utilized to find the binding affinity between protein and drug in the four complexes. All frames (∼1000 frame) were used in this calculation for each protein-ligand complex. The binding energy (Kcal/mol) produced from the MM-GBSA analysis with the standard deviation as error bars revealed TMPRSS2_camostat complex (–53.5059 Kcal/mol) had the best binding affinity (Figure 15).

The cluster representatives for each trajectory with the number of bonds between the drug and the protein are shown in Table 7. Compared to camostat, cryptospirolepine in the representative cluster displayer week interaction with TMPRSS2, and this coincides with the MM-GBSA results (Figures 15–17). The most common interactions are hydrophobic interactions in case of ACE2_cryptospirolepine complex, while the predominant interaction was hydrogen bond in TMPRSS2_Camostat complex. Figures 16–19 show the first and last representative frame (whenever possible) of the complexes.

3.5. Pharmacokinetic properties of selected alkaloids

Five of the best docked alkaloids: cryptospirolepine, 10-hydroxyusambarensine, cryptoquindoline, isocryptolepine, and strychnopentamine (Figure 20) fulfilled the requirement for Lipinski analysis of the rule of-five with corresponding favorable predicted ADME/tox parameters (Table 8). The physicochemical and pharmacokinetics analyses suggested these five alkaloids (Figure 20) have a high probability of absorption, subcellular distribution, except for AMES toxicity

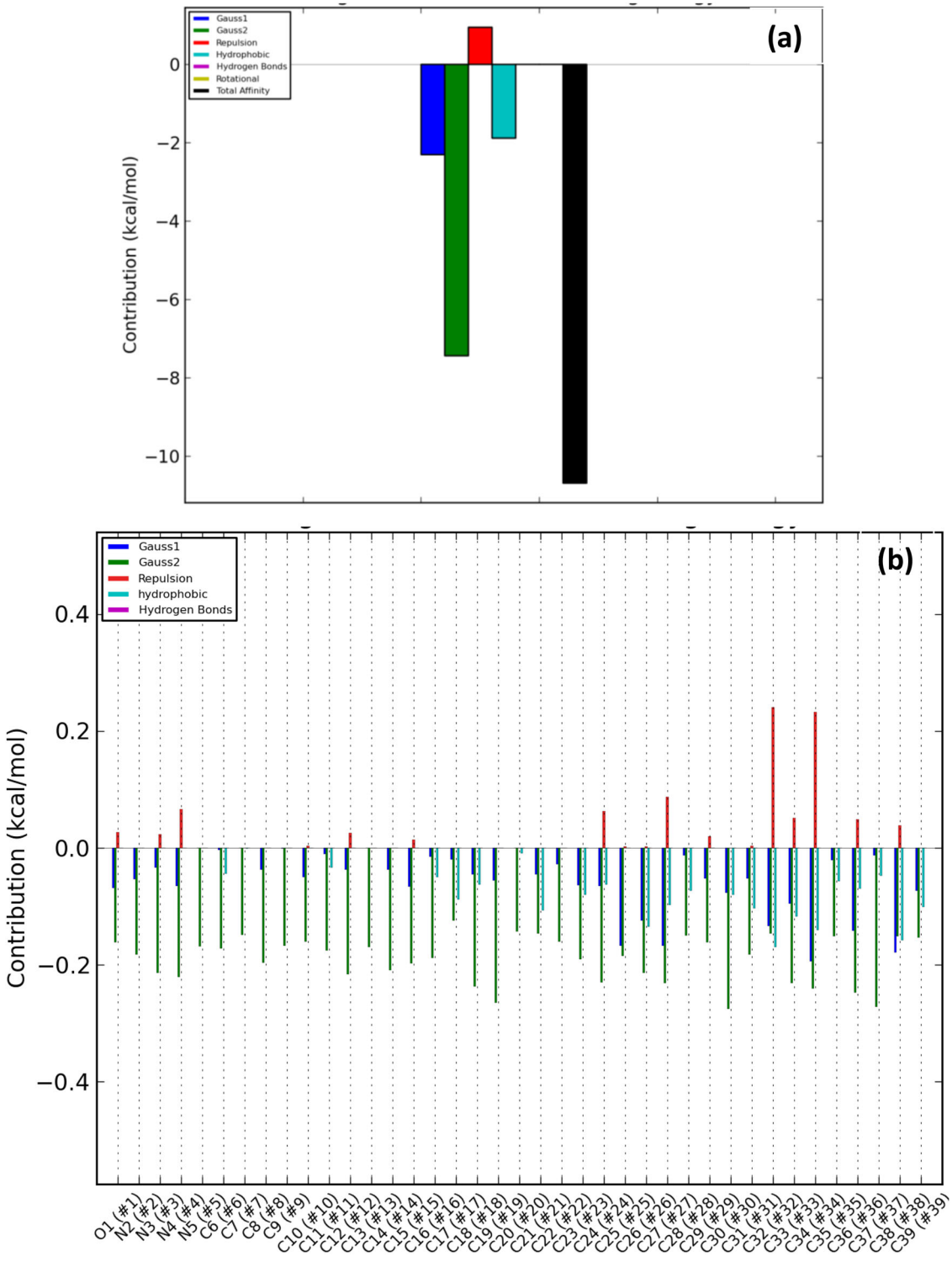

Figure 8. Overall energy profile of cryptospirolepine binding groups in SARS-Cov-2 spike glycoprotein: (a) Energetic contribution to the binding and (b) Energetic contributions for each atom in the ligand.

parameter which indicated cryptoquindoline to be toxic at a probability of 0.89. All the top docked alkaloids were indicated to be non-carcinogenic, with very low acute toxicity and aqueous solubility of <0. The gastrointestinal absorption index was indicated to be high for 10–hydroxyusambarensine, isocryptolepine and 6-oxoisoiguesterin but low for cryptospirolepine and cryptoquindoline (Table 8).

4. Discussion

Recognition of receptor on the host cell by coronavirus is obligatory for infection to occur. Both SARS-CoV and SARS-CoV-2 have been reported to utilize sites on ACE2 of the human cell as receptor (Hoffmann et al., 2020). The massive surface area of the lung, and the vast distribution of ACE2 in human alveolar epithelial cells makes the lungs a vulnerable

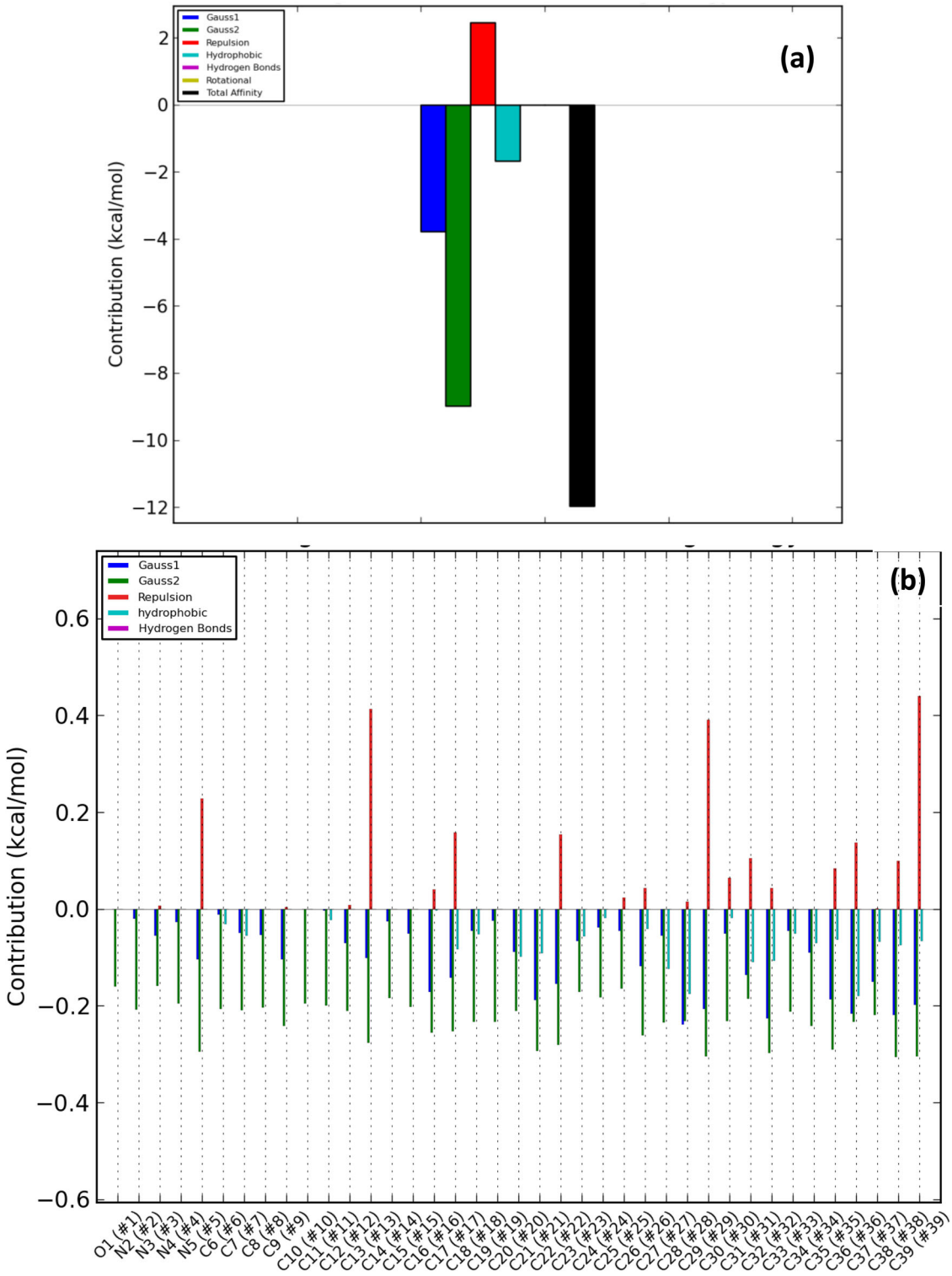

Figure 9. Overall energy profile of cryptospirolepine binding groups in SARS-CoV spike glycoprotein: (a) Energetic contribution to the binding energy and (b) Energetic contributions for each atom in the ligand.

target organ for the virus (Zhao et al., 2020). Thus, compounds that hinder viral entry into cell, or directly disrupt viral replication processes will halt transmissibility and pathogenicity. Blocking the cell entry effectively ensures the virus is denied access to host cell mechanism for replication. We hypothesized that alkaloids from African medicinal plants with reported bioactivity including antiviral potentials may interrupt coronavirus cell entry and consequently halt viral replication, pathogenicity, and transmissibility. To understand this, we evaluated the virtual binding of the alkaloids to the coronavirus spike glycoprotein, human ACE2, TMPRSS2, and the complex formed between the spike glycoprotein RBD and ACE2 (ACE2-RBD).

Computer modeling reveals the spike glycoproteins of SARS-CoV and SARS-CoV-2 have about 80% amino acid similarity (Li et al., 2005; Xia et al., 2020; Xu et al., 2020). The

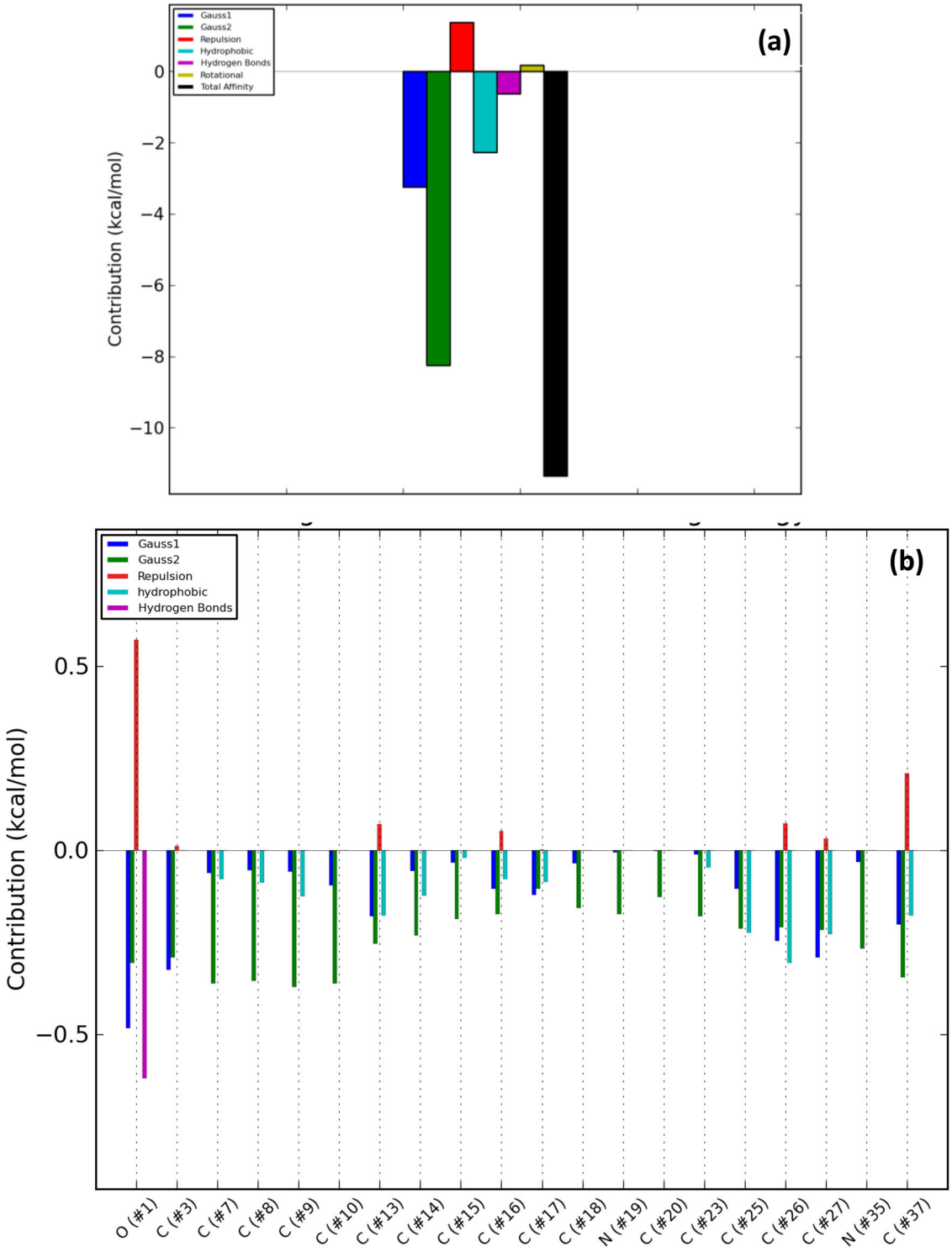

Figure 10. Overall energy profile of 10 –Hydroxyusambarensine binding groups in MERS-CoV spike glycoprotein: (a) Energetic contribution to the binding energy and (b) Energetic contributions for each atom in the ligand.

receptor binding domain (RBD) in the spike glycoproteins of SARSCoV and SARSCoV-2 are similar, with a root mean square deviation (RMSD) of about 0.68 Å over 139 pairs of Cα atoms (Yan et al., 2020). The spike glycoprotein is a type I fusion protein. In addition to binding to the receptor with S_1 subunit, it uses S_2 subunit to facilitate fusion of viral envelope with host cell membrane (Tong, 2009; Zhou et al., 2020). These two domains could be therapeutic targets. The top 20 alkaloids demonstrated good binding affinities to the spike glycoprotein. Cryptospirolepine, isocryptolepine, cryptoquindoline, and 10-hydroxyusambarensine had better binding to the spike glycoprotein of SARS-CoV-2, SARS-CoV, and MERS-CoV compared to the reference compound nafamostat. The binding strength of cryptospirolepine to the coronaviruses was consistently better than that of other alkaloids except for 10-hydroxyusambarensine that slightly demonstrated better binding to the spike glycoprotein of MERS-CoV. The interactions of these alkaloids with the spike

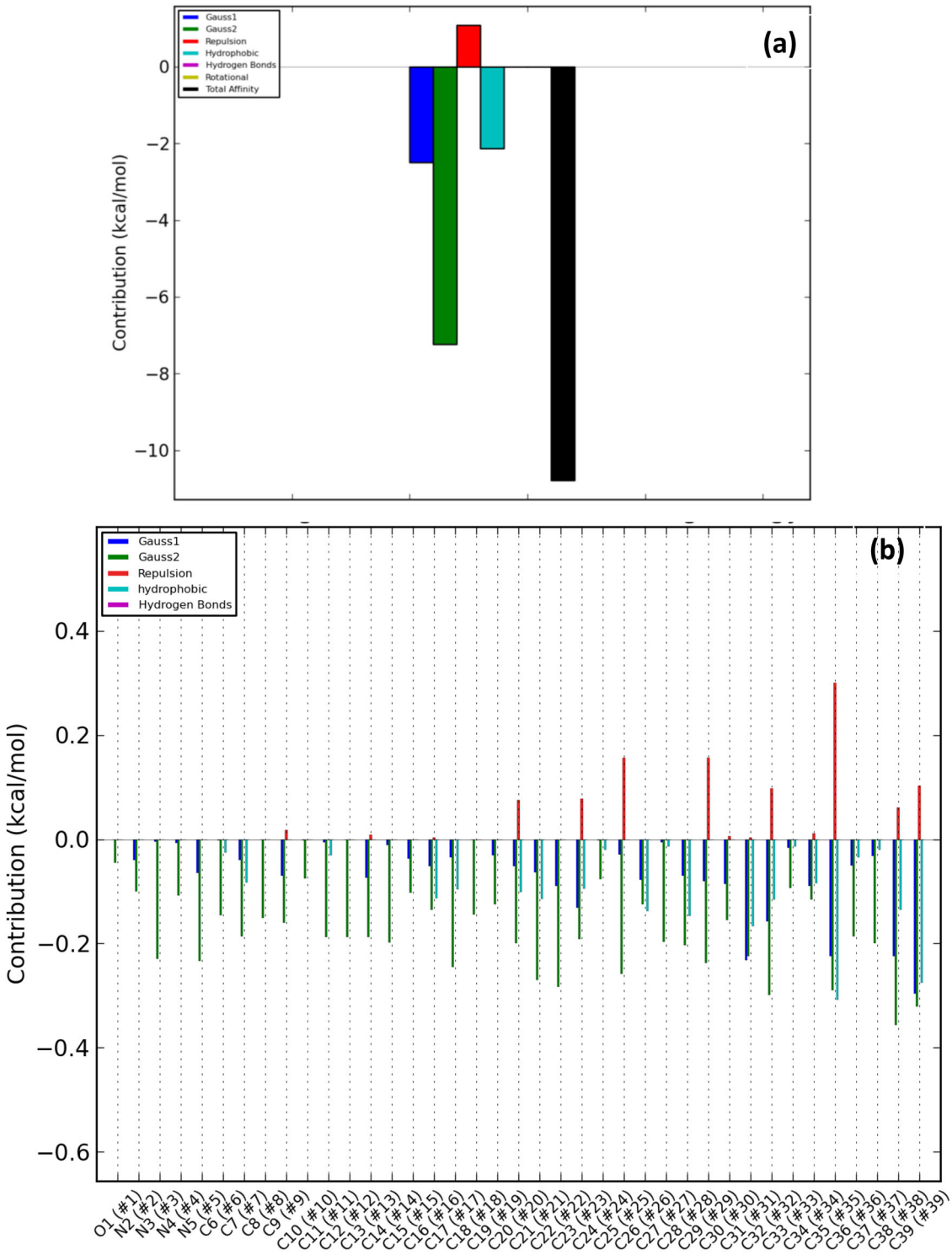

Figure 11. Overall energy profile of Cryptospirolepine binding groups in human ACE2: (a) Energetic contribution to the binding energy and (b) Energetic contributions for each atom in the ligand.

glycoprotein could alter the stabilizing effects that Leu[455], Gln[493], and Asn[501] in the RBD offers to the hotspots of ACE2. Also, the insertion of Phe[486] from SARS-CoV-2 RBD into the hydrophobic pocket (Shang et al., 2020) may be hindered, thereby weakening the possible interaction of SARS-CoV-2 RBD with ACE2. The strong binding affinities of these alkaloids for spike glycoproteins suggest their capacity to alter the conformation of the spike glycoproteins of these coronaviruses and halt their binding to host receptor.

Compounds that bind ACE2 have potential to block the interactions of SARS-CoV-2 and SARS-CoV. ACE2 is a receptor essential for viral cell entry. SARS-CoV-2 and SARS-CoV have been reported to utilize ACE2 as functional cell receptor (Hoffmann et al., 2020; Li et al., 2003; Wan et al., 2020; Zhou et al., 2020) but the spike glycoprotein of SARS-CoV-2 was reported to have more than 10 times higher binding affinity compared with SARS-CoV (Wrapp et al., 2020). This high affinity of SARS-CoV-2 for ACE2 appears to contribute to the

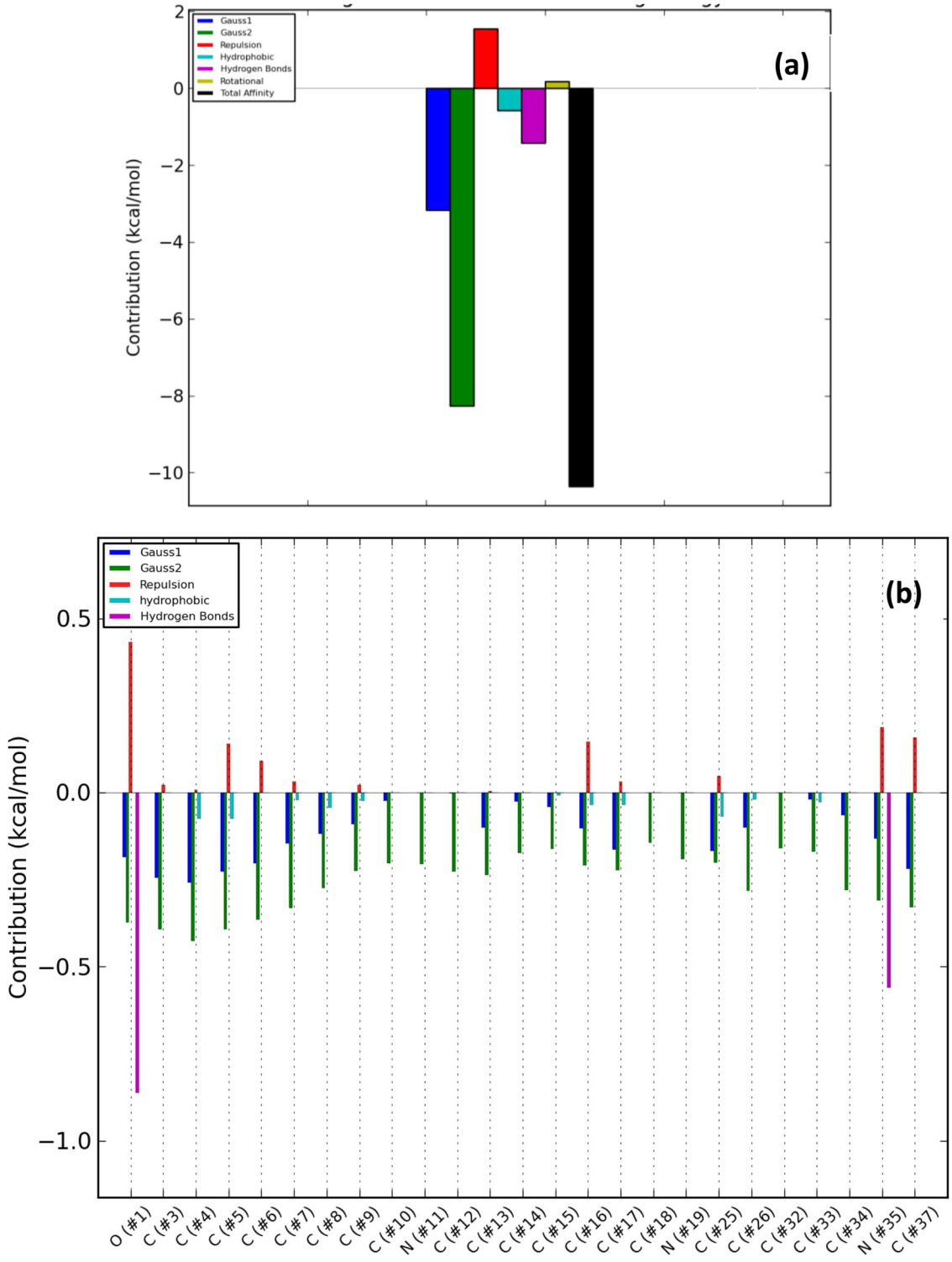

Figure 12. Overall energy profile of Cryptospirolepine binding groups in human TMPRSS2: (a) Energetic contribution to the binding energy and (b) Energetic contributions for each atom in the ligand.

efficient human to human transmission of the virus, and the rate at which it infects cells. The multiple binding of SARS-CoV to the receptor results in down regulation of ACE2 expression, thereby causing reduced protective mechanism of ACE2 against lung injury (Imai et al., 2005; Kuba et al., 2005), and enhanced renin-angiotensin pathway which favors tissue injury through ACE: these make the virus lethal. SARS-CoV spike protein binds strongly with human ACE2 (Li et al., 2005); Glutamine (residue 479) in the receptor-binding domain (RBD) of SARS-CoV which corresponds to residue 394 in SARS-CoV-2 (Wan et al., 2020) binds to essential lysine 31 on the human ACE2 receptor (Wu et al., 2012). The interactions of SARS-coronaviruses with ACE2 are similar. Each peptidase domain of ACE2 accommodates one receptor binding domain in S_1 subunit of spike protein. This interaction is mediated mainly through polar interactions (Song et al., 2018; Yan et al., 2020). However, the receptor binding domain in S_1 subunit of SARS-CoV and SARS-CoV-2 are

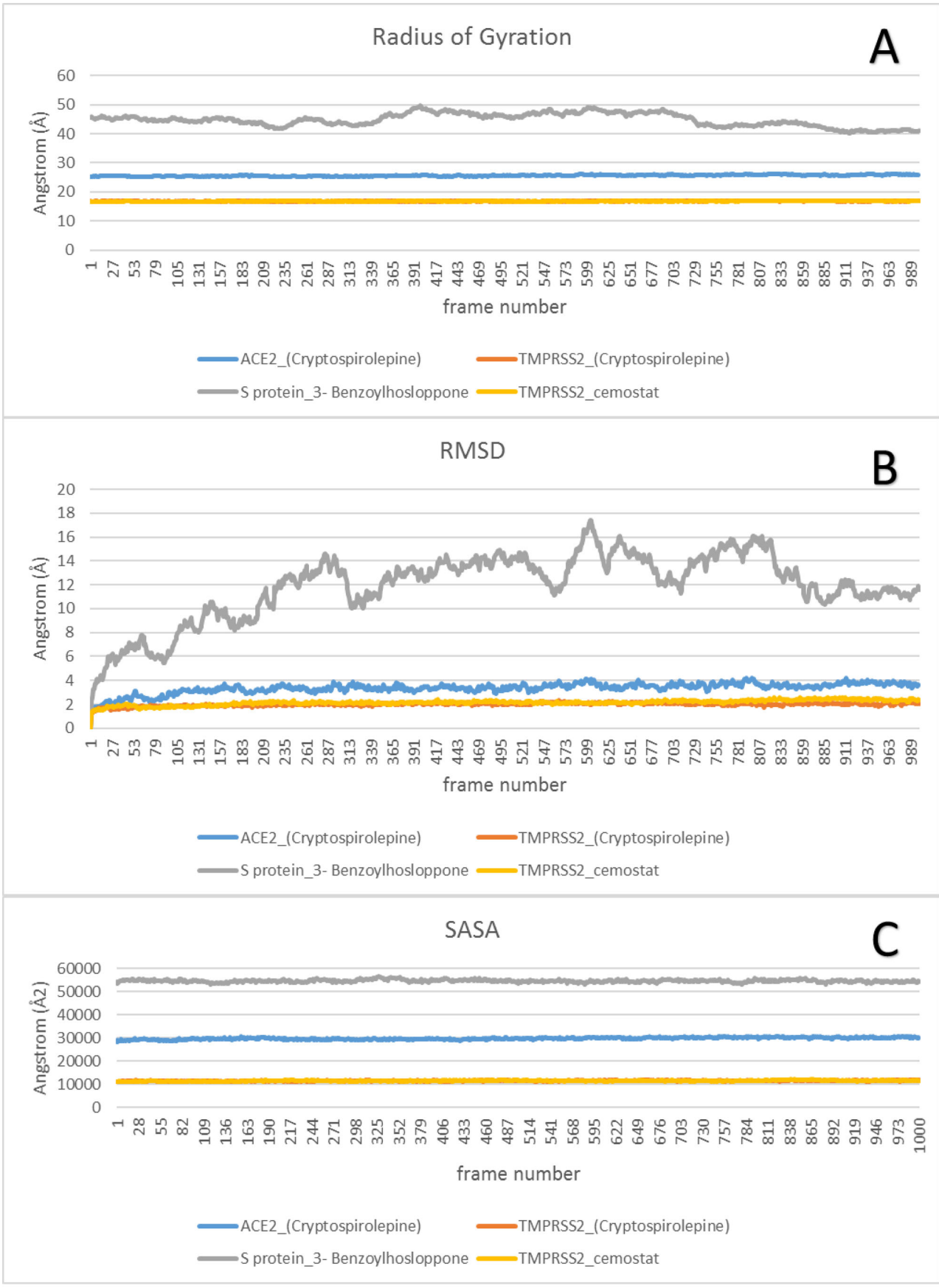

Figure 13. The Radius of Gyration (RoG), Root Mean Square Deviation (RMSD), and Surface Accessible Surface Area (SASA) for each of protein-ligand complex.

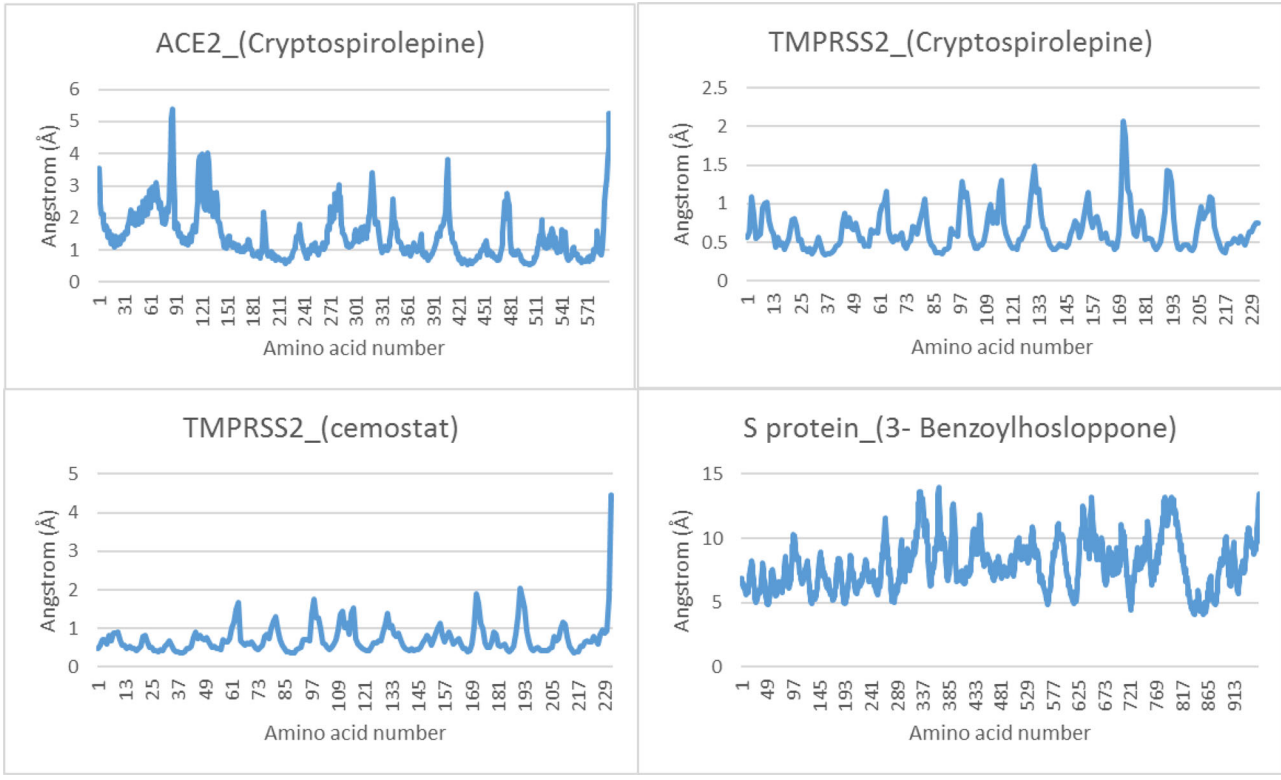

Figure 14. The Root Mean Square Fluctuation for ACE2_(Cryptospirolepine), TMPRSS2_(Cryptospirolepine), TMPRSS2_(Camostat), and S glycoprotein_(3-Benzoylhosloppone), respectively. The spikes at the end of TMPRSS2_camostat, and ACE2_(Cryptospirolepine) corresponds to the motion of the terminals.

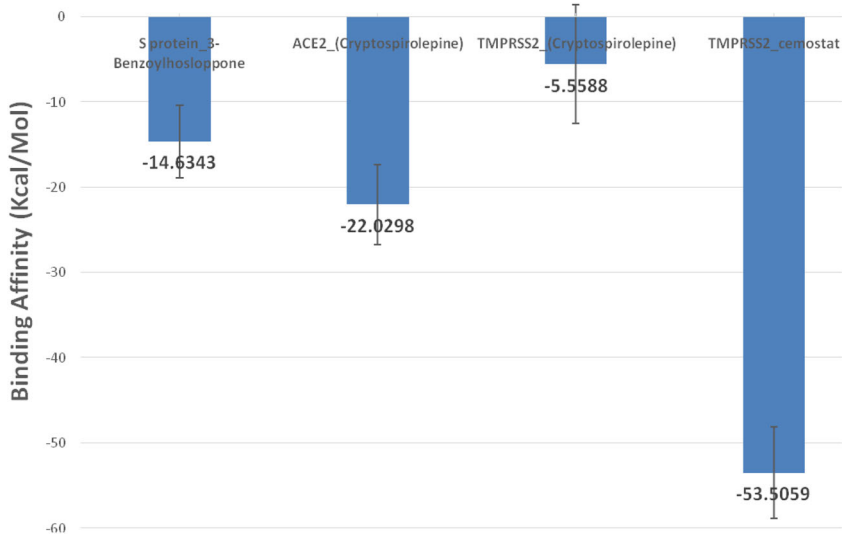

Figure 15. The binding energy and standard deviation in (Kcal/mol) produced from the MM-GBSA analysis.

reported to show sequence and conformational variations in their interfaces with ACE2: variations at the N terminus of α1 where Arg^{426}, Tyr^{484}, and Thr^{487} in SARS-CoV are respectively replaced by Asn^{439}, Gln^{498}, and Asn^{501} in SARS-CoV-2; variation at the C terminus of α1 where Leu^{472} in SARS-CoV is replaced by Phe^{486} in SARS-CoV-2 (Yan et al., 2020); and the replacement of Tyr^{442} and Asn^{479} in SARS-CoV by Leu^{455} and Gln^{493} respectively in SARS-CoV-2 (Walls et al., 2020). These variations appear to be responsible for the difference in affinity of these coronaviruses for ACE2. The affinity of the viral spike glycoprotein for the host cellular receptor dictates binding. Alteration of this affinity limits viral nucleocapsid access to the host cytosol. This alteration can be achieved by changing the conformation of the host cell receptor, or direct binding of the spike glycoprotein by chemical agents. The binding affinities of reference compounds (MLN-4760 and N-Acetyl-d-glucosamine) for ACE2 was lesser relative to the alkaloids cryptospirolepine, 10-Hydroxyusambarensine, and strychnopentamine which have binding energy of −10.7, −10.4, and −9.9 Kcal/mol, respectively. The stronger binding of these alkaloids to ACE2 could alter the receptor. Lys^{31} and Lys^{353} are reported as the hotspots of ACE2, essential for the binding of coronavirus (Li et al., 2005; Shang et al., 2020). Interactions of compounds with this region is

Table 7. Clusters, its representative frame and the protein-ligand complexes interactions.

TMPRSS2_ camostat complex				
Cluster number (representative frame)	Hydrophobic	Hydrogen bond	Salt-bridges	Pi-cation
Cluster 1 (frame 92)	None	**A190** (2) Q192 **D217** E218 A220	**D189**	**H57**
Cluster 2 (frame 618)	Q192–V213	R41 **A190** S195 **D217** E218	H57–**D189**	**None**
Cluster 3 (frame 284)	Q192	**A190** (2) S195 **D217** (2)	**D189**	**None**
Cluster 4 (frame 728)	None			
Cluster 5 (frame 915)	Q192			
TMPRSS2_(Cryptospirolepine) complex				
Cluster number (representative frame)	Hydrophobic	Pi-stacking	Pi-cation	
Cluster 1 (frame 747)	No Interactions			
Cluster 2 (frame 121)	Y149(2)	None	R41	
Cluster 3 (frame 515)	No Interactions			
Cluster 4 (frame 966)	P28, H119	W207	None	
Cluster 5 (frame 699)	No Interactions			
ACE2_(Cryptospirolepine) complex				
Cluster number (representative frame)	Hydrophobic	Hydrogen bond	Pi-stacking	
Cluster 1 (Frame 39)	L73, L100, F390, L391	None	None	
Cluster 2 (Frame157)	L39, **F40** (2), **W69**, L73, F390 (2), L391	N394	**F40**, **W69**	
Cluster 3 (Frame433)	L39, **F40** (2), **W69** (3), L73, A99, F390 (2)	None	**F40**, **W69**	
Cluster 4 (Frame736)	**F40**, **W69** (2), L73, L100, F390 (2)	None	**F40**, **W69**	
Cluster 5 (Frame843)	**F40**, L73, F390	None	**W69**	
S protein_(3-Benzoylhosloppone) complex				
Cluster number (representative frame)	Hydrophobic	Hydrogen bond	Pi-stacking	
Cluster 1 (Frame316)	Y38, E224, P225	Y38	**F43**	
Cluster 2 (Frame577)	**F43**	None	**F43**	

The amino acids in bold are the most common in each complex.

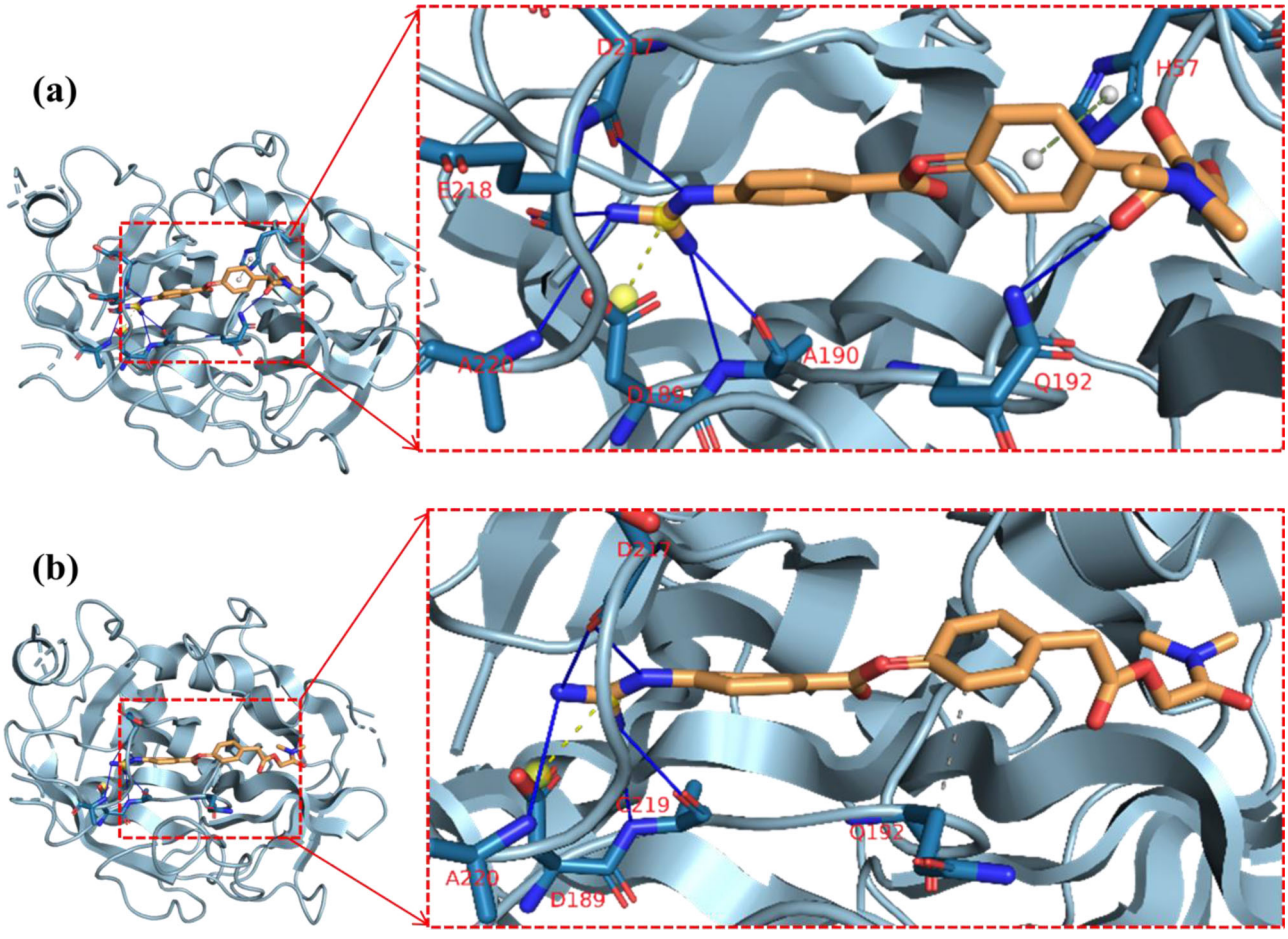

Figure 16. The representative structure for each cluster for TMPRSS2_Camostat and the types of interactions. Gray-dotted line is hydrophobic interactions, blue lines are hydrogen bond interactions, yellow-dotted lines represent salt-bridges, and green-dotted lines represent pi-stacking interactions. Single-letter amino acids are in red color. (a) Cluster 1 representative frame: 92 (b) Cluster 5 representative frame: 915.

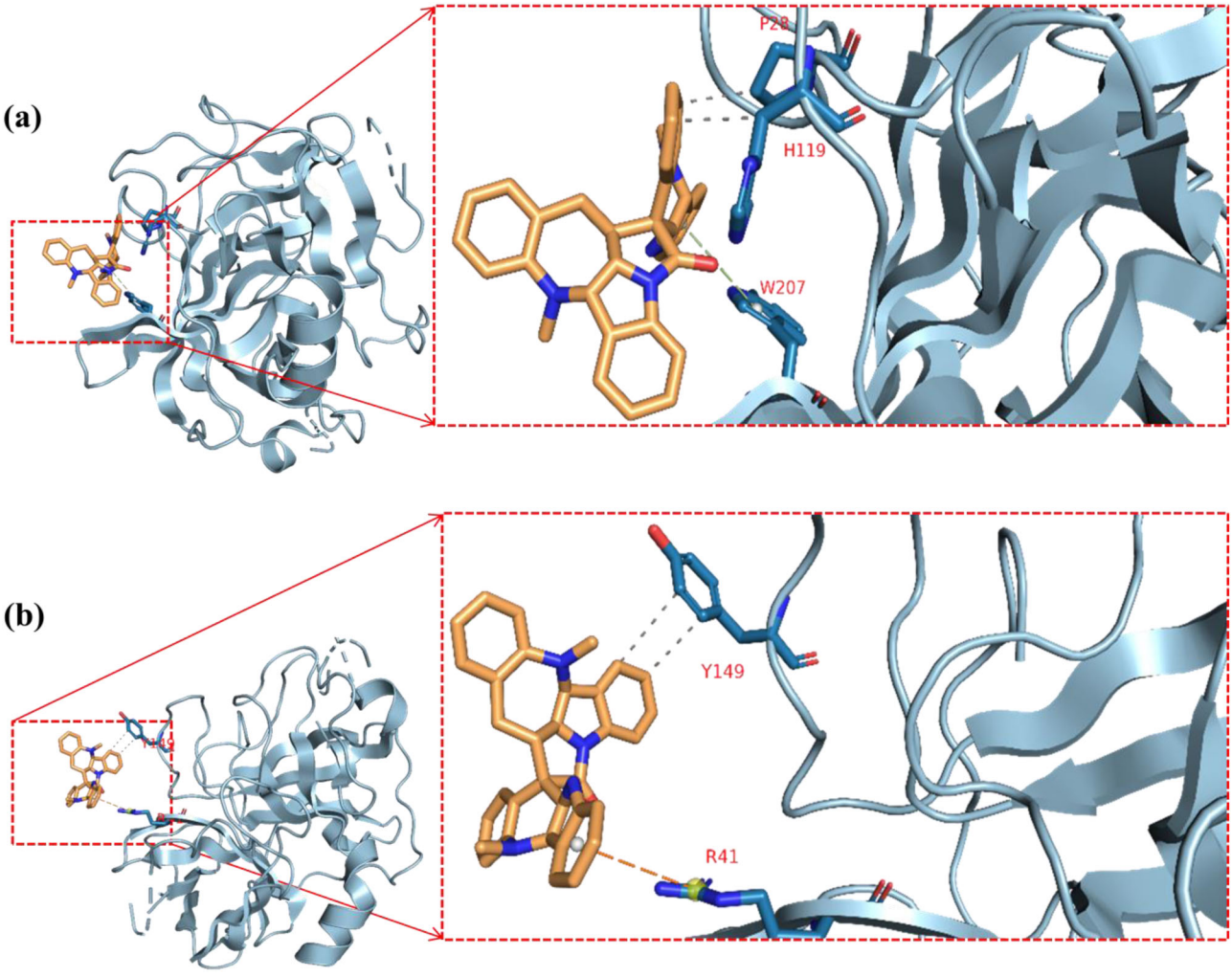

Figure 17. The second and fourth clusters in TMPRSS2_(Cryptospirolepine) complex. Gray-dotted line represents hydrophobic interactions, orange-dotted lines represent pi-cation interactions, and green-dotted lines represent pi-stacking interactions. Single-letter amino acids are in red color. (a) Cluster 2 Representative frame: 121 and (b) Cluster 4 representative frame: 966.

proposed to affect the binding of coronavirus (Gaunt et al., 2010). The interaction of these alkaloids with adjacent residues rather than the hotspots of ACE2 suggest the ability of the alkaloids to alter the suitable hydrophobic environment that is needed for coronavirus binding. This possible alteration may halt the interaction of RBD of the spike glycoprotein with ACE2.

In addition to the ability of alkaloids to block access to ACE2, we tested the possibility of them binding to the complex formed between the spike glycoprotein RBD and ACE2 (ACE2-RBD). From the list of alkaloids, cryptospirolepine, 10–hydroxyusambarensine, and chrysopentamine demonstrated best binding with ACE2-RBD, with binding energy of −10.7, −10.5, and −10.5 Kcal/mol. These alkaloids affinities for ACE2-RBD indicate that cryptospirolepine, 10–hydroxyusambarensine, and chrysopentamine may disrupt cell entry of SARS-CoV-2 even at the point when the S_1 subunit of spike glycoprotein binds to ACE2. Stabilization of the interface between RBD of SARS-CoV-2 and human ACE2 is essential, and achieved by coronavirus by its residues at the RBD. The hotspots (Lys^{31} and Lys^{353}) on ACE2 need to be suitably accommodated in hydrophobic setting for effective binding of coronavirus. To achieve this, SARS-CoV-2 neutralizes the charges of lysine residues by stabilizing Lys^{31} of ACE2 with Leu^{455} and Gln^{493}, and further stabilizing Lys^{353} of ACE2 by Asn^{501} (Shang et al., 2020). These contribute to favorable recognition of ACE2 receptor. Both cryptospirolepine and 10–hydroxyusambarensine, by their interactions, may be good candidates to block access of spike glycoprotein to ACE2, and destabilize the ACE2-RBD complex.

TMPRSS2 is a member of the human type II transmembrane protease serine which is defined by N-terminal transmembrane domain, and a C-terminal extracellular serine protease domain. The spike glycoprotein of SARS-CoV and SARS-CoV-2 are reported to be primed by host protease TMPRSS2 (Glowacka et al., 2011; Hoffmann et al., 2020); an essential step for fusion of viral and host cell membranes. The S_2 subunit in the spike glycoprotein of SARS-CoV-2 appears to facilitate fusion of viral envelope with host cell membrane better than that of SARS-CoV (Xia et al., 2020). This promotes entry of viral content into host cell cytoplasm. Inhibiting this fusion will also limit the viral spread. *In vitro* study reveals that blocking the activity of TMPRSS2 inhibits cell entry of SARS-CoV (Kawase et al., 2012). The SARS-CoV-2 spike protein has several multi-basic arginine residues at the S_1/S_2 cleavage site. This indicates a high tendency of cleavage at this point

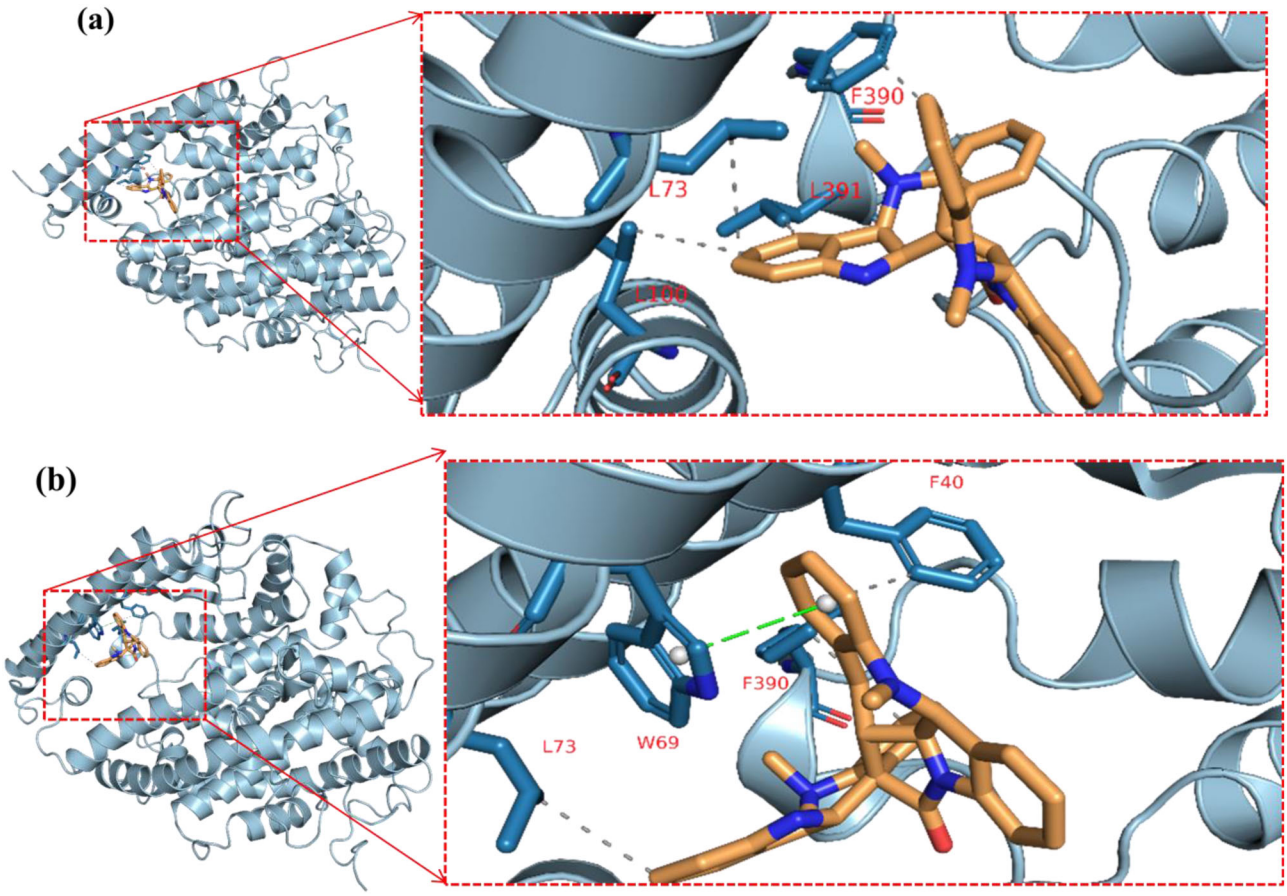

Figure 18. The first and last clusters in ACE2_(Cryptospirolepine) complex. Gray-dotted line represents hydrophobic interactions, and green-dotted lines represent pi-stacking interactions. Single-letter amino acids are in red color. (a) Cluster 1 representative frame: 39 and (b) Cluster 5 Representative frame: 843.

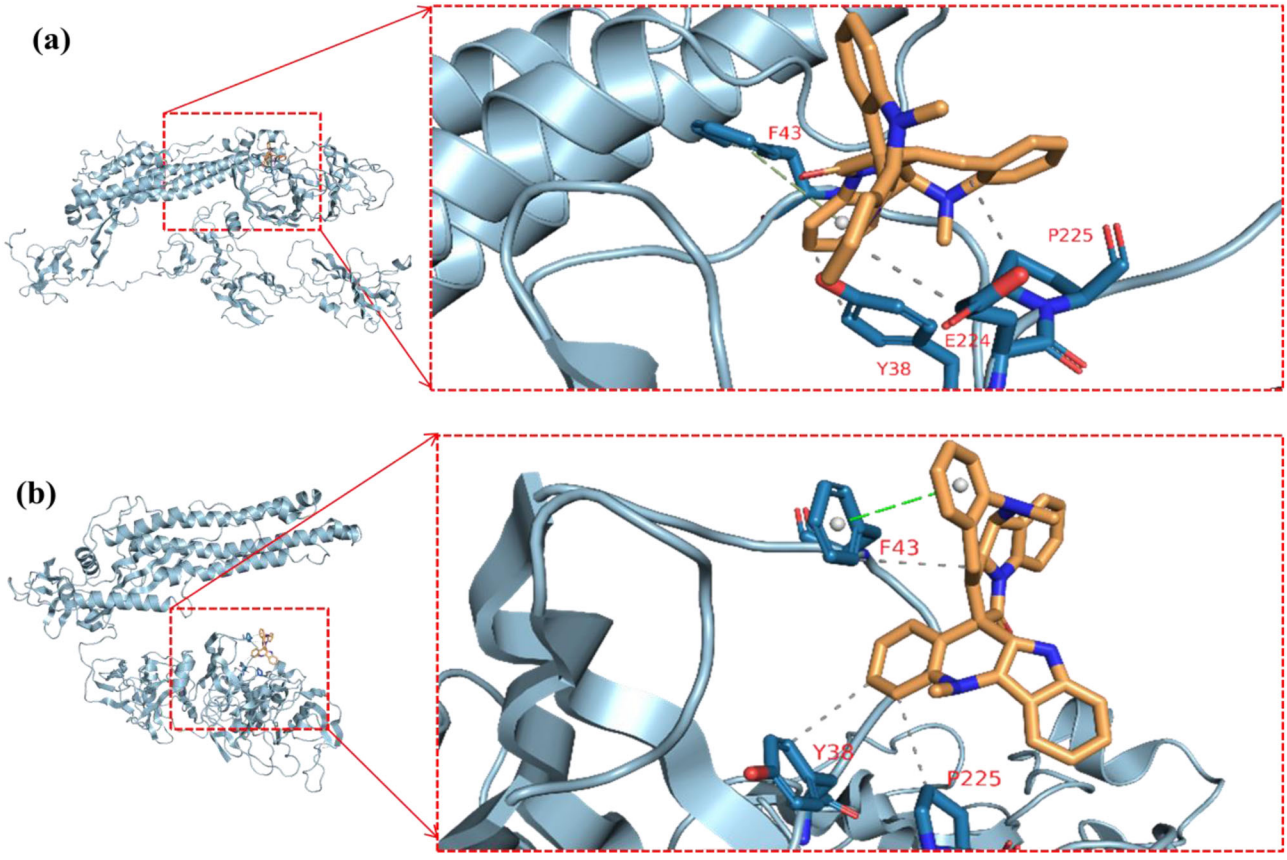

Figure 19. The first and last clusters in spike glycoprotein_(3-Benzoylhosloppone) complex. Gray-dotted line represent hydrophobic interactions, blue lines represents hydrogen bond interactions, and green-dotted lines represent pi-stacking interactions. (a) Cluster 1 representative frame: 316 and (b) Cluster 3 Representative frame: 772.

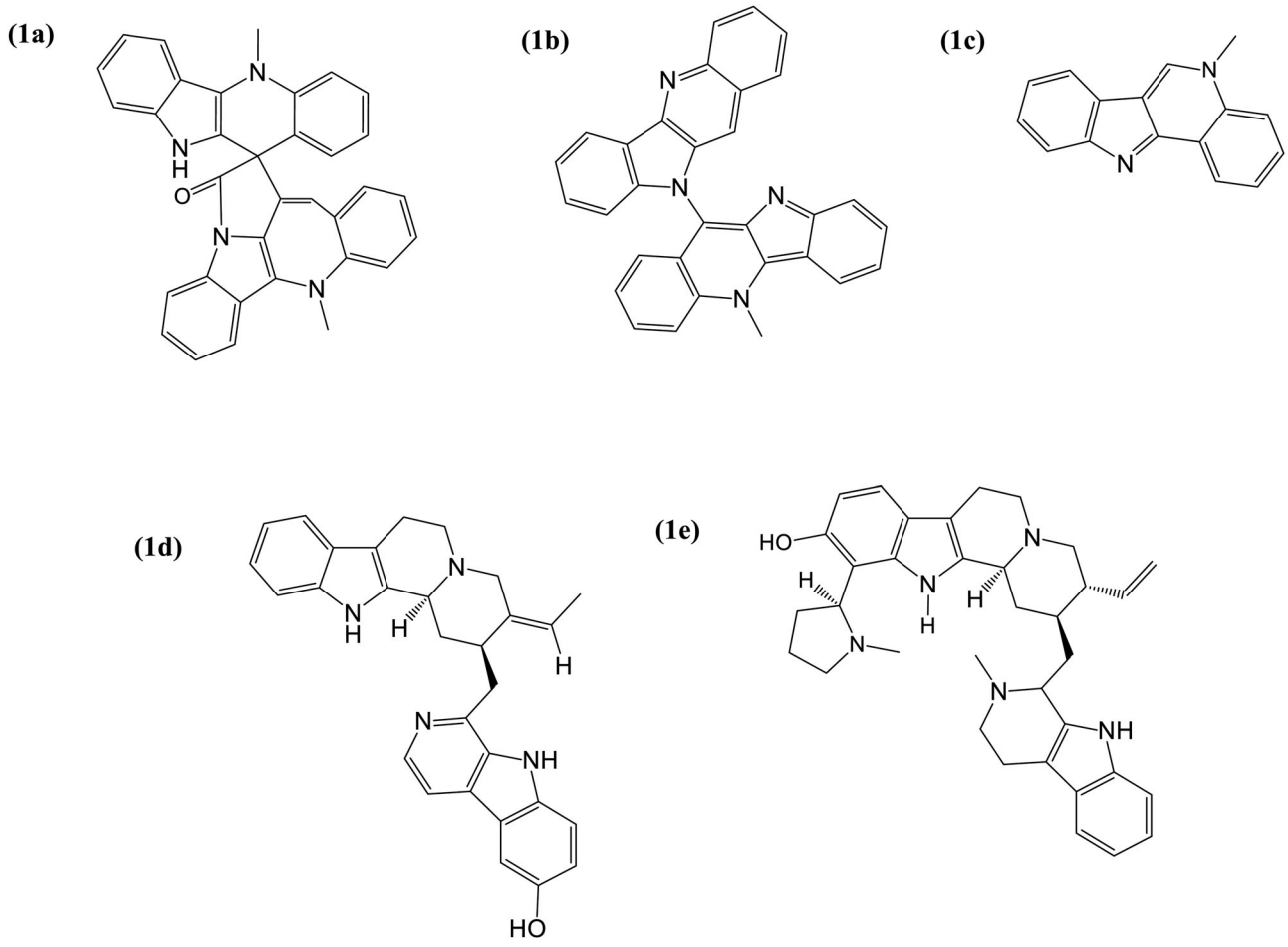

Figure 20. Structure of alkaloids with highest binding affinity to ACE2, TMPRSS2 and SARS-CoV-2 spike glycoprotein (a) Cryptospirolepine, (b) Cryptoquindoline, (c) Isocryptolepine, (d) 10–Hydroxyusambarensine, and (e) Strychnopentamin.

(Hoffmann et al., 2020). Report suggests that annulment of the S_1/S_2 cleavage site in the spike glycoprotein of SARS-CoV-2 affects its mediated cell entry (Walls et al., 2020). This indicates the importance of the cleavage performed by the host cell protease TMPRSS2, as the cleavage activates fusion of viral and host cell membranes, to guarantee viral infectiveness. The alkaloids 10–hydroxyusambarensine, cryptospirolepine, and cryptoquindoline demonstrated binding energy of −10.4, −9.9, and −9.7 Kcal/mol, respectively to the host protease TMPRSS2. These affinities were better than the binding provided by the reference compound (camostat). Camostat mesylate, a serine protease inhibitor, was reported to block the activity of TMPRSS2 (Zhou et al., 2015) and compounds with similar antiviral activity could be considered as anti-SARS-CoV-2 (Yamamoto et al., 2016). While 10–hydroxyusambarensine had the best binding affinity, it interacted in similar manner as camostat: both were docked into the S_1-specificity pocket of TMPRSS2. Both compounds interacted with residue Ala^{190}, Asp^{189} and Gln^{192} which are amino acid located at the basement of the pocket. This essential interaction with Asp^{189} determines the specificity of the S_1 pocket for basic residues Arg and Lys of the substrate (Kyrieleis et al., 2007). The amidino nitrogen and hydroxyl group of 9H-pyrido[3,4-b]indol-6-ol moiety of 10–hydroxyusambarensine were responsible for the hydrogen bond with the protein. Similar to the phenylquanidine of camostat, the 9H-pyrido[3,4-b]indol-6-ol moiety of 10–hydroxyusambarensine, with its hydroxyl group directed towards the carboxylate group of Asp^{189}, formed strong hydrogen bond with Asp^{189} and other residue in the pocket. The phenyl group of the 9H-pyrido[3,4-b]indol-6-ol further had hydrophobic interactions with CYS^{119} and TRP^{215}, just as the peptide planes of the bonds between Trp^{215}–Gly^{216} and Cys^{191}–Gln^{192} sandwiched the phenyl ring of benzamidine in the native ligand to TMPRSS2 (Kyrieleis et al., 2007). Apart from the 9H-pyrido[3,4-b]indol-6-ol moiety, other groups of 10–hydroxyusambarensine interacted with the imidazol ring of His^{57} of the S_2 pocket that is found next to the S_1 pocket and ARG^{41} which are outside the hydrophobic cleft. A similar interaction was observed with camostat. The additional hydrophobic interaction by 10–hydroxyusambarensine may be responsible for its higher binding affinity relative to camostat. In a similar docking study with SARS-CoV-2 3CLpro, 10–hydroxyusambarensine, cryptospirolepine, and cryptoquindoline were observed to be docked in strikingly similar pattern as ritonavir with even higher binding affinities (Gyebi et al., 2020). The interaction of these alkaloids with TMPRSS2 may limit its protease function, thereby preventing the fusion of viral and human cell membranes. The potential exhibited by 10–hydroxyusambarensine, cryptospirolepine, and cryptoquindoline to inhibit the cleavage of spike

Table 8. *In silico* prediction of physicochemical and pharmacokinetics properties of top binding alkaloids.

(a) Lipinski filter analysis					
Lipinski filters	Cryptospirolepine	10-Hydroxyusambarensine	Cryptoquindoline	Isocryptolepine	Strychnopentamine
Molecular weight (g/mol)	504.58	448.56	448.52	232.28	459.75
Num. heavy atoms	39	34	35	18	41
Num. rotatable bonds	2	2	1	0	4
Num. H-bond acceptors	1	3	2	1	4
Hydrogen bond donor	1	3	0	0	3
cLogP	3.75	3.31	4.02	4.02	3.51
Molar refractivity	161.96	142.46	145.65	76.01	180.14
Lipinski violation	1	0	0	0	1
(b) Admet SAR					
Absorption (Probability)					
Blood-Brain Barrier	BBB+ (0.99)	BBB+ (0.83)	BBB+ (0.95)	BBB+ (0.97)	BBB+ (0.71)
Human intestinal absorption	HIA+ (0.97)	HIA+ (0.98)	HIA+ (0.99)	HIA+ (0.99)	HIA+ (0.98)
Bioavailability score	0.55	0.55	0.55	0.55	0.55
Caco-2 permeability	Caco2+ (0.74)	Caco2+ (0.53)	Caco2+ (0.76)	Caco2+ (0.67)	Caco2+ (0.53)
P-glycoprotein substrate	Nonsubstrate (0.50)	Substrate (0.91)	Noninhibitor (0.69)	Noninhibitor (0.74)	Noninhibitor (0.87)
P-glycoprotein inhibitor	Noninhibitor (0.84)	Noninhibitor (0.60)	Noninhibitor (0.72)	Noninhibitor (0.74)	Noninhibitor (0.54)
Renal organic cation transporter	Noninhibitor (0.70)	Inhibitor (0.80)	Noninhibitor (0.67)	Noninhibitor (0.54)	Noninhibitor (0.70)
Distribution (Probability)					
Subcellular localization	Mitochondria (0.70)	Mitochondria (0.65)	Mitochondria (0.55)	Mitochondria (0.76)	Mitochondria (0.57)
Metabolism					
CYP450 Substrate	Substrate (0.69) Noninhibitor (0.76)	Substrate (0.53) Noninhibitor (0.83)	Substrate (0.86) Noninhibitor (0.86)	Substrate (0.65) Noninhibitor (0.81)	Nonsubstrate (0.79) Inhibitor (0.54)
Toxicity					
AMES toxicity	Non AMES toxic (0.61)	Non AMES toxic (0.75)	AMES toxic (0.89)	AMES toxic (0.80)	Non AMES toxic (0.68)
Carcinogens	Noncarcinogens (0.94)	Noncarcinogens (0.97)	Noncarcinogens (0.92)	Noncarcinogens (0.96)	Noncarcinogens (0.95)
Acute oral toxicity	III (0.50)	III (0.51)	III (0.67)	III (0.72)	III (0.56)
Rat acute toxicity LD_{50} (mol/kg)	2.4992	2.7896	2.4420	2.3770	2.7631
Aqueous solubility (LogS)	−3.5692	−2.7626	−3.1120	−3.21	−2.6192
Pharmacokinetics					
GI absorption	Low	High	Low	High	High
Log K_p (skin permeation) (cm/s)	−4.82	−5.70	−3.97	−5.38	−5.82

glycoprotein by interacting with TMPRSS2, suggest they may function as inhibitors of SARS-CoV-2 cell entry. The result from the MDS analysis of the top docked alkaloids with their complexed proteins showed that the complexes were stable and could be therefore subjected to experimental processes in further studies. The Lipinski filtering analysis showed that these five alkaloids are drug-like, with no more than one violation of Lipinski's rule (Lipinski et al., 1997). Likewise, the predicted ADMET filtering evaluation shows that these alkaloids may be well absorbed, distributed, metabolized, and not toxic. Though 10–hydroxyusambarensine may be more absorbed in the gastrointestinal tract than cryptospirolepine. However, these alkaloids may be optimized more to improve their physicochemical and pharmacokinetics properties.

5. Conclusion

In summary, this study provides evidence that alkaloids from Africa medicinal plants may disrupt cell entry of SARSCoV-2 by binding to the spike glycoprotein, by blocking the human cell receptor ACE2, and inhibiting the host cell serine protease TMPRSS2 utilized by SARS-CoV-2 for spike glycoprotein priming. Given the capacity to interact with the proteins essential for receptor-binding and membrane fusion, cryptospirolepine, 10-hydroxyusambarensine, and cryptoquindoline could serve as pan-SARS-coronavirus cell entry inhibitors. These alkaloids could serve as essential inhibitors to prevent and/or treat COVID-19, and other coronavirus diseases that may emerge in future.

Disclosure statement

No potential conflict of interest was reported by the authors.

Funding

This study was not funded.

References

Aanouz, I., Belhassan, A., & El-Khatabi, K. (2020). Moroccan medicinal plants as inhibitors against SARS-CoV-2 main protease: Computational investigations. *Journal of Biomolecular Structure and Dynamics*, 1–9.

Adeoye, A. O., Oso, B. J., & Olaoye, I. F. (2020). Repurposing of chloroquine and some clinically approved antiviral drugs as effective therapeutics to prevent cellular entry and replication of coronavirus. *Journal of Biomolecular Structure and Dynamics*, 1–14.

Al-Tawfiq, J. A., & Memish, Z. A. (2014). Middle East respiratory syndrome coronavirus: Transmission and phylogenetic evolution. *Trends in Microbiology*, *22*(10), 573–579. https://doi.org/10.1016/j.tim.2014.08.001

Bertram, S., Heurich, A., Lavender, H., Gierer, S., Danisch, S., Perin, P., Lucas, J. M., Nelson, P. S., Pöhlmann, S., & Soilleux, E. J. (2012). Influenza and SARS-coronavirus activating proteases TMPRSS2 and HAT are expressed at multiple sites in human respiratory and gastrointestinal tracts. *PloS One*, *7*(4), e35876. https://doi.org/10.1371/journal.pone.0035876

Bolles, M., Donaldson, E., & Baric, R. (2011). SARS-CoV and emergent coronaviruses: Viral determinants of interspecies transmission. *Current Opinion in Virology*, *1*(6), 624–634. https://doi.org/10.1016/j.coviro.2011.10.012

Boopathi, S., Poma, A. B., & Kolandaivel, P. (2020). Novel 2019 Coronavirus structure, mechanism of action, antiviral drug promises and rule out against its treatment. *Journal of Biomolecular Structure and Dynamics*, 1–14.

Brooks, B. R., Brooks, C. L., Mackerell, A. D., Nilsson, L., Petrella, R. J., Roux, B., Won, Y., Archontis, G., Bartels, C., Boresch, S., Caflisch, A., Caves, L., Cui, Q., Dinner, A. R., Feig, M., Fischer, S., Gao, J., Hodoscek, M., Im, W., … Karplus, M. (2009). CHARMM: The biomolecular simulation program. *Journal of Computational Chemistry*, *30*(10), 1545–1614. https://doi.org/10.1002/jcc.21287

Cabeça, T. K., Granato, C., & Bellei, N. (2013). Epidemiological and clinical features of human coronavirus infections among different subsets of patients. *Influenza and Other Respiratory Viruses*, *7*(6), 1040–1047. https://doi.org/10.1111/irv.12101

Case, D., Belfon, K., & Ben-Shalom, I. (2020). AMBER 2020.

Cheng, F., Li, W., Zhou, Y., Shen, J., Wu, Z., Liu, G., Lee, P. W., & Tang, Y. (2012). AdmetSAR: A comprehensive source and free tool for assessment of chemical ADMET properties. *Journal of Chemical Information and Modeling*, *52*(11), 3099–3105. https://doi.org/10.1021/ci300367a

Dhama, K., Karthik, K., Khandia, R., Munjal, A., Tiwari, R., Rana, R., Khurana, S. K., Ullah, S., Khan, R. U., Alagawany, M., & Farag, M. R. (2018). Medicinal and therapeutic potential of herbs and plant metabolites/extracts countering viral pathogens-current knowledge and future prospects. *Current Drug Metabolism*, *19*(3), 236–263. https://doi.org/10.2174/1389200219666180129145252

Elmezayen, A. D., Al-Obaidi, A., & Şahin, A. T. (2020). Drug repurposing for coronavirus (COVID-19): in silico screening of known drugs against coronavirus 3CL hydrolase and protease enzymes. *Journal of Biomolecular Structure and Dynamics*, 1–12.

Gallagher, T. M., & Buchmeier, M. J. (2001). Coronavirus spike proteins in viral entry and pathogenesis. Virology, *279*(2), 371–374. https://doi.org/10.1006/viro.2000.0757

Gaunt, E. R. R., Hardie, A., Claas, E. C. C. J., Simmonds, P., & Templeton, K. E. E. (2010). Epidemiology and clinical presentations of the four human coronaviruses 229E, HKU1, NL63, and OC43 detected over 3 years using a novel multiplex real-time PCR method. *Journal of Clinical Microbiology*, *48*(8), 2940–2947. https://doi.org/10.1128/JCM.00636-10

Glowacka, I., Bertram, S., Müller, M. A., Allen, P., Soilleux, E., Pfefferle, S., Steffen, I., Tsegaye, T. S., He, Y., Gnirss, K., Niemeyer, D., Schneider, H., Drosten, C., & Pöhlmann, S. (2011). Evidence that TMPRSS2 activates the severe acute respiratory syndrome coronavirus spike protein for membrane fusion and reduces viral control by the humoral immune response. *Journal of Virology*, *85*(9), 4122–4134. https://doi.org/10.1128/JVI.02232-10

Gorbalenya, A. E., Baker, S. C., & Baric, R. S. (2020). The species Severe acute respiratory syndrome-related coronavirus: Classifying 2019-nCoV and naming it SARS-CoV-2. *Nature Microbiology 5*(4), 536–544.

Gyebi, A. G., Ogunro, B. O., Adegunloye, P. A., Ogunyemi, M. O., & Afolabi, O. S. (2020). Potential inhibitors of Coronavirus 3-Chymotrypsin-Like Protease ($3CL^{pro}$): An *in silico* screening of alkaloids and terpenoids from African medicinal plants. *Journal of Biomolecular Structure and Dynamics*, (in press) https://doi.org/10.1080/7391102.2021764868

Heurich, A., Hofmann-Winkler, H., Gierer, S., Liepold, T., Jahn, O., & Pöhlmann, S. (2014). TMPRSS2 and ADAM17 cleave ACE2 differentially and only proteolysis by TMPRSS2 augments entry driven by the severe acute respiratory syndrome coronavirus spike protein. *Journal of Virology*, *88*(2), 1293–1307. https://doi.org/10.1128/JVI.02202-13

Hendaus, M. A. (2020). Remdesivir in the treatment of Coronavirus Disease 2019 (COVID-19): A simplified summary. *Journal of Biomolecular Structure and Dynamics*, 1–10.

Hoffmann, M., Kleine-Weber, H., Schroeder, S., Krüger, N., Herrler, T., Erichsen, S., Schiergens, T. S., Herrler, G., Wu, N.-H., Nitsche, A., Müller, M. A., Drosten, C., & Pöhlmann, S. (2020). SARS-CoV-2 cell entry depends on ACE2 and TMPRSS2 and is blocked by a clinically proven protease inhibitor. Cell, *181*(2), 271–280.e8. https://doi.org/10.1016/j.cell.2020.02.052

Humphrey, W., Dalke, A., & Schulten, K. (1996). VMD: Visual molecular dynamics. *Journal of Molecular Graphics*, *14*(1), 33–38. https://doi.org/10.1016/0263-7855(96)00018-5

Imai, Y., Kuba, K., Rao, S., Huan, Y., Guo, F., Guan, B., Yang, P., Sarao, R., Wada, T., Leong-Poi, H., Crackower, M. A., Fukamizu, A., Hui, C.-C., Hein, L., Uhlig, S., Slutsky, A. S., Jiang, C., & Penninger, J. M. (2005). Angiotensin-converting enzyme 2 protects from severe acute lung failure. Nature, *436*(7047), 112–116. https://doi.org/10.1038/nature03712

Kawase, M., Shirato, K., van der Hoek, L., Taguchi, F., & Matsuyama, S. (2012). Simultaneous treatment of human bronchial epithelial cells with serine and cysteine protease inhibitors prevents severe acute respiratory syndrome coronavirus entry. *Journal of Virology*, *86*(12), 6537–6545. https://doi.org/10.1128/JVI.00094-12

Khan, R. J., Jha, R. K., & Amera, G. (2020). Targeting SARS-Cov-2: A systematic drug repurposing approach to identify promising inhibitors against 3C-like proteinase and 2′-O-ribose methyltransferase. *Journal of Biomolecular Structure and Dynamics*, 1–40.

Kuba, K., Imai, Y., Rao, S., Gao, H., Guo, F., Guan, B., Huan, Y., Yang, P., Zhang, Y., Deng, W., Bao, L., Zhang, B., Liu, G., Wang, Z., Chappell, M., Liu, Y., Zheng, D., Leibbrandt, A., Wada, T., … Penninger, J. M. (2005). A crucial role of angiotensin converting enzyme 2 (ACE2) in SARS coronavirus-induced lung injury. *Nature Medicine*, *11*(8), 875–879. https://doi.org/10.1038/nm1267

Kudi, A. C., & Myint, S. H. (1999). Antiviral activity of some Nigerian medicinal plant extracts. *Journal of Ethnopharmacology*, *68*(1–3), 289–294. https://doi.org/10.1016/S0378-8741(99)00049-5

Kyrieleis, O. J. P., Huber, R., Ong, E., Oehler, R., Hunter, M., Madison, E. L., & Jacob, U. (2007). Crystal structure of the catalytic domain of DESC1, a new member of the type II transmembrane serine proteinase family. *The FEBS Journal*, *274*(8), 2148–2160. https://doi.org/10.1111/j.1742-4658.2007.05756.x

Lee, J., Cheng, X., Swails, J. M., Yeom, M. S., Eastman, P. K., Lemkul, J. A., Wei, S., Buckner, J., Jeong, J. C., Qi, Y., Jo, S., Pande, V. S., Case, D. A., Brooks, C. L., MacKerell, A. D., Klauda, J. B., & Im, W. (2016). CHARMM-GUI input generator for NAMD, GROMACS, AMBER, OpenMM, and CHARMM/OpenMM simulations using the CHARMM36 additive force field. *Journal of Chemical Theory and Computation*, *12*(1), 405–413. https://doi.org/10.1021/acs.jctc.5b00935

Letko, M., Marzi, A., & Munster, V. (2020). Functional assessment of cell entry and receptor usage for SARS-CoV-2 and other lineage B betacoronaviruses. *Nature Microbiology*, *5*(4), 562–568. https://doi.org/10.1038/s41564-020-0688-y

Li, F., Li, W., Farzan, M., & Harrison, S. C. (2005). Structure of SARS coronavirus spike receptor-binding domain complexed with receptor. *Science (New York, N.Y.)*, *309*(5742), 1864–1868. https://doi.org/10.1126/science.1116480

Li, W., Moore, M. J., Vasilieva, N., Sui, J., Wong, S. K., Berne, M. A., Somasundaran, M., Sullivan, J. L., Luzuriaga, K., Greenough, T. C., Choe, H., & Farzan, M. (2003). Angiotensin-converting enzyme 2 is a functional receptor for the SARS coronavirus. Nature, *426*(6965), 450–454. https://doi.org/10.1038/nature02145

Lipinski, C. A., Lombardo, F., Dominy, B. W., & Feeney, P. J. (1997). Experimental and computational approaches to estimate solubility and permeability in drug discovery and development settings. *Advanced Drug Delivery Reviews*, *23*(1–3), 3–25. https://doi.org/10.1016/S0169-409X(96)00423-1

Lobo-Galo, N., Terrazas-López, M., & Martínez-Martínez, A. (2020). FDA-approved thiol-reacting drugs that potentially bind into the SARS-CoV-2 main protease, essential for viral replication. *Journal of Biomolecular Structure and Dynamics*, 1–12.

Lu, R., Yu, X., Wang, W., Duan, X., Zhang, L., Zhou, W., Xu, J., Xu, L., Hu, Q., Lu, J., Ruan, L., Wang, Z., & Tan, W. (2012). Characterization of human coronavirus etiology in Chinese adults with acute upper respiratory tract infection by real-time RT-PCR assays. *PloS One.*, *7*(6), e38638. https://doi.org/10.1371/journal.pone.0038638

Meyer, J. J. M., Afolayan, A. J., Taylor, M. B., & Erasmus, D. (1997). Antiviral activity of galangin isolated from the aerial parts of *Helichrysum aureonitens*. *Journal of Ethnopharmacology*, *56*(2), 165–169. https://doi.org/10.1016/S0378-8741(97)01514-6

Miller, B. R., McGee, T. D., Swails, J. M., Homeyer, N., Gohlke, H., & Roitberg, A. E. (2012). MMPBSA.py: An efficient program for end-state free energy calculations. *Journal of Chemical Theory and Computation*, *8*(9), 3314–3321. https://doi.org/10.1021/ct300418h

Morris, G. M., Huey, R., Lindstrom, W., Sanner, M. F., Belew, R. K., Goodsell, D. S., & Olson, A. J. (2009). AutoDock4 and AutoDockTools4: Automated docking with selective receptor flexibility. *Journal of Computational Chemistry*, *30*(16), 2785–2791. https://doi.org/10.1002/jcc.21256

Muralidharan, N., Sakthivel, R., & Velmurugan, D. (2020). Computational studies of drug repurposing and synergism of lopinavir, oseltamivir and ritonavir binding with SARS-CoV-2 Protease against COVID-19. *Journal of Biomolecular Structure and Dynamics*, 1–7.

O'Boyle, N. M., Banck, M., James, C. A., Morley, C., Vandermeersch, T., & Hutchison, G. R. (2011). Open Babel: An open chemical toolbox. *Journal of Cheminformatics*, *3*(1), 33 https://doi.org/10.1186/1758-2946-3-33

Ogbole, O. O., Akinleye, T. E., Segun, P. A., Faleye, T. C., & Adeniji, A. J. (2018). In vitro antiviral activity of twenty-seven medicinal plant extracts from Southwest Nigeria against three serotypes of echoviruses. *Virology Journal*, *15*(1), 110. https://doi.org/10.1186/s12985-018-1022-7

Paules, C. I., Marston, H. D., & Fauci, A. S. (2020). Coronavirus infections-more than just the common cold. JAMA, *323*(8), 707–708. https://doi.org/10.1001/jama.2020.0757

Phillips, J. C., Braun, R., Wang, W., Gumbart, J., Tajkhorshid, E., Villa, E., Chipot, C., Skeel, R. D., Kalé, L., & Schulten, K. (2005). Scalable molecular dynamics with NAMD. *Journal of Computational Chemistry*, *26*(16), 1781–1802. https://doi.org/10.1002/jcc.20289

Salentin, S., Schreiber, S., Haupt, V. J., Adasme, M. F., & Schroeder, M. (2015). PLIP: Fully automated protein-ligand interaction profiler. *Nucleic Acids Research*, *43*(W1), W443–W447. https://doi.org/10.1093/nar/gkv315

Sánchez-Linares, I., Pérez-Sánchez, H., Cecilia, J. M., & García, J. M. (2012). High-Throughput parallel blind virtual screening using BINDSURF. *BMC Bioinformatics*, *13*(Suppl 14), S13. https://doi.org/10.1186/1471-2105-13-S14-S13

Shang, J., Ye, G., Shi, K., Wan, Y., Luo, C., Aihara, H., Geng, Q., Auerbach, A., & Li, F. (2020). Structural basis of receptor recognition by SARS-CoV-2. Nature, *581*(7807), 221–224. https://doi.org/10.1038/s41586-020-2179-y

Shulla, A., Heald-Sargent, T., Subramanya, G., Zhao, J., Perlman, S., & Gallagher, T. (2011). A transmembrane serine protease is linked to the severe acute respiratory syndrome coronavirus receptor and activates virus entry. *Journal of Virology*, *85*(2), 873–882. https://doi.org/10.1128/JVI.02062-10

Simmons, G., Zmora, P., Gierer, S., Heurich, A., & Pöhlmann, S. (2013). Proteolytic activation of the SARS-coronavirus spike protein: Cutting enzymes at the cutting edge of antiviral research. *Antiviral Research*, *100*(3), 605–614. https://doi.org/10.1016/j.antiviral.2013.09.028

Song, W., Gui, M., Wang, X., & Xiang, Y. (2018). Cryo-EM structure of the SARS coronavirus spike glycoprotein in complex with its host cell receptor ACE2. *PLoS Pathogens*, *14*(8), e1007236. https://doi.org/10.1371/journal.ppat.1007236

Tong, T. R. (2009). Drug targets in severe acute respiratory syndrome (SARS) virus and other coronavirus infections. *Infectious Disorder Drug Targets*, *9*(2), 223–245. https://doi.org/10.2174/187152609787847659

Towler, P., Staker, B., Prasad, S., Menon, S., Tang, J., Parsons, T., Ryan, D., Fisher, M., Williams, D., Dales, N., Patane, M., & Pantoliano, M. (2004). ACE2 X-ray structures reveal a large hinge-bending motion important for inhibitor binding and catalysis. *The Journal of Biological Chemistry*, *279*(17), 17996–18007. https://doi.org/10.1074/jbc.M311191200

Trott, O., & Olson, A. J. (2010). AutoDock Vina: Improving the speed and accuracy of docking with a new scoring function, efficient optimization, and multithreading. *Journal of Computational Chemistry*, *31*(2), 455–461. https://doi.org/10.1002/jcc

Tubiana, T., Carvaillo, J.-C., Boulard, Y., & Bressanelli, S. (2018). TTClust: A versatile molecular simulation trajectory clustering program with graphical summaries. *Journal of Chemical Information and Modeling*, *58*(11), 2178–2182. https://doi.org/10.1021/acs.jcim.8b00512

Walls, A. C., Park, Y. J., Tortorici, M. A., Wall, A., McGuire, A. T., & Veesler, D. (2020). Structure, function, and antigenicity of the SARS-CoV-2 spike glycoprotein. Cell, *181*(2), 281–212. https://doi.org/10.1016/j.cell.2020.02.058

Walsh, E. E., Shin, J. H., & Falsey, A. R. (2013). Clinical impact of human coronaviruses 229E and OC43 infection in diverse adult populations. *The Journal of Infectious Diseases*, *208*(10), 1634–1642. https://doi.org/10.1093/infdis/jit393

Wan, Y., Shang, J., Graham, R., Baric, R. S., Ralph, S., & Li, F. (2020). Receptor recognition by the Novel Coronavirus from Wuhan: An analysis based on decade-long structural studies of SARS coronavirus. *Journal of Virology*, *94*(7), e00127. https://doi.org/10.1128/JVI.00127-20

WHO (2020). *Report of the WHO-China joint mission on coronavirus disease 2019 (COVID-19).* https://www.who.int/docs/default-source/coronaviruse/who-china-joint-mission-on-covid-19-final-report.pdf

Wrapp, D., Wang, N., Corbett, K. S., Goldsmith, J. A., Hsieh, C. L., Abiona, O., Graham, B. S., & McLellan, J. S. (2020). Cryo-EM structure of the 2019-nCoV spike in the prefusion conformation. *Science (New York, N.Y.)*, *367*(6483), 1260–1263. https://doi.org/10.1126/science.aax0902

Wu, K., Peng, G., Wilken, M., Geraghty, R. J., & Li, F. (2012). Mechanisms of host receptor adaptation by severe acute respiratory syndrome coronavirus. *The Journal of Biological Chemistry*, *287*(12), 8904–8911. https://doi.org/10.1074/jbc.M111.325803

Xia, S., Liu, M., Wang, C., Xu, W., Lan, Q., Feng, S., Qi, F., Bao, L., Du, L., Liu, S., Qin, C., Sun, F., Shi, Z., Zhu, Y., Jiang, S., & Lu, L. (2020). Inhibition of SARS-CoV-2 (previously 2019-nCoV) infection by a highly potent pan-coronavirus fusion inhibitor targeting its spike protein that harbors a high capacity to mediate membrane fusion . *Cell Research*, *30*(4), 343–355. https://doi.org/10.1038/s41422-020-0305-x

Xu, X., Chen, P., Wang, J., Feng, J., Zhou, H., Li, X., Zhong, W., & Hao, P. (2020). Evolution of the novel coronavirus from the ongoing Wuhan outbreak and modeling of its spike protein for risk of human transmission. *Science China: Life Sciences*, *63*(3), 457–460. https://doi.org/10.1007/s11427-020-1637-5

Yamamoto, M., Matsuyama, S., Li, X., Takeda, M., Kawaguchi, Y., Inoue, J. I., & Matsuda, Z. (2016). Identification of nafamostat as a potent inhibitor of middle east respiratory syndrome Coronavirus s protein-mediated membrane fusion using the split-protein-based cell-cell fusion assay. *Antimicrobial Agents and Chemotherapy*, *60*(11), 6532–6539. https://doi.org/10.1128/AAC.01043-16

Yan, R., Zhang, Y., Li, Y., Xia, L., Guo, Y., & Zhou, Q. (2020). Structural basis for the recognition of SARS-CoV-2 by full-length human ACE2. *Science (New York, N.Y.)*, *367*(6485), 1444–1448. https://doi.org/10.1126/science.abb2762

Yuan, Y., Cao, D., Zhang, Y., Ma, J., Qi, J., Wang, Q., Lu, G., Wu, Y., Yan, J., Shi, Y., Zhang, X., & Gao, G. F. (2017). Cryo-EM structures of MERS-CoV and SARS-CoV spike glycoproteins reveal the dynamic receptor binding domains. *Nature Communications*, *8*(1), 1–9. https://doi.org/10.1038/ncomms15092

Zhang, H., Penninger, J. M., Li, Y., Zhong, N., & Slutsky, A. S. (2020). Angiotensin-converting enzyme 2 (ACE2) as a SARS-CoV-2 receptor: Molecular mechanisms and potential therapeutic target. *Intensive Care Medicine*, *46*(4), 586–585. https://doi.org/10.1007/s00134-020-05985-9

Zhao, Y., Zhao, Z., Wang, Y., Zhou, Y., Ma, Y., & Zuo, W. (2020). Single-cell RNA expression profiling of ACE2, the putative receptor of Wuhan 2019-nCov. *BioRxiv*, https://doi.org/10.1101/2020.01.26.919985

Zhou, P., Yang, X.-L., Wang, X.-G., Hu, B., Zhang, L., Zhang, W., Si, H.-R., Zhu, Y., Li, B., Huang, C.-L., Chen, H.-D., Chen, J., Luo, Y., Guo, H., Jiang, R.-D., Liu, M.-Q., Chen, Y., Shen, X.-R., Wang, X., … Shi, Z.-L. (2020). A pneumonia outbreak associated with a new coronavirus of probable bat origin. Nature, *579*(7798), 270–274. https://doi.org/10.1038/s41586-020-2012-7

Zhou, Y., Vedantham, P., Lu, K., Agudelo, J., Carrion, R., Nunneley, J. W., Barnard, D., Pöhlmann, S., McKerrow, J. H., Renslo, A. R., & Simmons, G. (2015). Protease inhibitors targeting coronavirus and filovirus entry. *Antiviral Research*, *116*, 76–84. https://doi.org/10.1016/j.antiviral.2015.01.011